

Review

Recent Development of Electrolyte Engineering for Sodium Metal Batteries

Yingying Ji ¹, Jiabao Li ² and Jinliang Li ^{1,*} 

¹ Siyuan Laboratory, Guangzhou Key Laboratory of Vacuum Coating Technologies and New Energy Materials, Guangdong Provincial Engineering Technology Research Center of Vacuum Coating Technologies and New Materials, Department of Physics, Jinan University, Guangzhou 510632, China

² School of Chemistry and Chemical Engineering, Yangzhou University, 180 Si-Wang-Ting Road, Yangzhou 225002, China

* Correspondence: lijinliang@email.jnu.edu.cn

Abstract: Intermittent renewable energy requires a powerful energy storage system to smoothen the relationship between power generation and power consumption. Due to the rapidly rising price of Li resources, the development of Li-ion batteries (LIBs) has been severely limited. Therefore, developing high-efficiency and low-cost Na-ion batteries has become an alternative to energy storage systems. The high potential plateau of most anode materials urges the exploration of the ultimate anode, the Na metal anode. However, three big dilemmas regarding Na metal anodes, including the formation of Na dendrites, the formation of dead Na, and the continuous appearance of bare Na lead to the degradation of the performance of Na metal batteries (NMBs). In this review, we mainly summarize the recent progress to address these dilemmas for NMBs by electrolyte optimization. We firstly discuss the liquid electrolyte progresses to improve the Na metal anode's electrochemical performance by solvent chemistry, salt chemistry, and additive. In addition, considering the ultimate goal of NMBs is solid-state batteries, we also discuss the recent progress of polymer electrolytes and all-solid-state electrolytes for Na metal anodes and summarize the enhancement of Na-ion transport mechanisms and interface engineering mechanisms of different solid-state electrolytes. Furthermore, the critical challenges and new perspectives of NMBs using electrolyte optimization are also emphasized. We believe that our review will provide insight to conduct more comprehensive and effective electrolyte engineering for high-performance NMBs.



Citation: Ji, Y.; Li, J.; Li, J. Recent Development of Electrolyte Engineering for Sodium Metal Batteries. *Batteries* **2022**, *8*, 157. <https://doi.org/10.3390/batteries8100157>

Academic Editor: Claudio Gerbaldi

Received: 8 September 2022

Accepted: 30 September 2022

Published: 4 October 2022

Publisher's Note: MDPI stays neutral with regard to jurisdictional claims in published maps and institutional affiliations.



Copyright: © 2022 by the authors. Licensee MDPI, Basel, Switzerland. This article is an open access article distributed under the terms and conditions of the Creative Commons Attribution (CC BY) license (<https://creativecommons.org/licenses/by/4.0/>).

1. Introduction

Recently, energy shortage has become a major challenge faced by today's society. The development of alternative renewable energy including wind energy and solar energy has become the current mainstream [1–3]. However, most of the alternative renewable energy appears as intermittent energy due to natural conditions, resulting in efficient energy storage systems being required to store and integrate this energy into the grid [4–7]. The lithium (Li) ion battery (LIB) has become the choice of the current energy storage system due to its high efficiency and stability [8–10]. However, with the rapid expansion of the energy storage market, the price of Li resources has also risen rapidly, indicating that LIBs will not be able to meet the demand for large-scale electrical energy storage applications in the future [11–14]. Therefore, exploring low-cost electrochemical energy storage systems has become the goal of future grid energy storage.

Due to the similar operating principle to LIB and low-cost sodium (Na) resource, the Na ion battery (NIB) also receives lots of attention and is supposed to be the next generation low-cost battery for the large-scale energy storage system [15–17]. However, the NIBs practical applications are severely limited by the development of anode materials because graphite as the most successful commercial anode for LIBs presented poor Na-storage

performance due to the mismatch between the large ion radius of Na^+ and the relatively narrow interlayer distance ($<0.37 \text{ nm}$) [18–21]. The development of high-performance NIB anodes becomes an urgent issue. At present, researchers have developed a series of anodes for NIBs, including hard carbon, oxides, sulfides, etc. [22–25]. However, consideration of the high electrochemical redox potential and high redox potential will result in the low energy density in the Na-ion full battery. Thus, it is urgent to develop an anode with a low potential for NIBs. Compared with current conventional NIB anodes, Na metal anodes can present extremely low working potential and higher theoretical specific capacity, which become the best choice of NIB anodes [26,27]. Therefore, the development of Na metal anodes with high stability and safety is of great significance for realizing high energy density NIBs. Nevertheless, the practical application of Na metal anodes faces enormous challenges in terms of stability, safety, and reversibility [21,28]. Firstly, the organic electrolyte will decompose to a certain extent, and the solid electrolyte interface (SEI) layer will be formed on the Na metal surface when the organic electrolyte contacts the Na metal anodes [29–31]. Since the SEI layer exhibits a porous and loose structure and unstable composition, Na metal penetrates the SEI layer and deposits beneath the SEI layer during the Na plating process. With the continuous plating/stripping process, the Na metal will arise in a series of deposition and dissolution courses. This behavior leads to the fracture of the loose SEI layer, resulting in the appearance of bare Na metal in the anode [32,33]. A new SEI layer will be formed in the bare Na metal, aggravating the consumption of organic electrolytes. Secondly, the non-uniform electric field exists due to the rough electrodes during the plating process, resulting in the non-uniform Na metal deposition, which facilitates the formation of Na dendrites [34–36]. The dendrite growth increases the surface area of the Na metal and aggravates side reactions between the Na metal and the electrolyte. With the continuous growth of Na dendrites, the separator is eventually pierced, which leads to the short circuit of the NIBs and causes serious safety hazards [37,38]. Short circuits are often accompanied by thermal runaway of the batteries, which can even result in battery combustion and explosion. Thirdly, after the Na dendrites grow during the plating process, part of the Na metal is easily dissolved from the roots of the dendrites first in the subsequent Na stripping process [39,40]. This behavior causes the separation of stem ends of the Na dendrites and Na metal anodes, triggering the loss of electron transfer channels, which is regarded as “dead Na” [41,42]. With the continuous increase in dead Na, the Na metal anode is severely depleted, which causes a sharp decrease in diffusion kinetics [43,44]. This dead Na leads to high resistance, resulting in increased polarization and reduced energy efficiency. In addition, the volume change for Na metal anodes is infinitely higher than that of conventional anodes during the Na plating/stripping process. The problem of volume change is exacerbated by dendrite growth. The corresponding schemes are shown in Figure 1a. These dilemmas all lead to the degradation of the performance of Na metal anodes.

To solve these issues, researchers have developed various strategies for the stabilization of Na metal anodes. To sum up, it mainly includes three parts (Figure 1b). Firstly, by modifying the deposition substrate of the Na metal anodes, the homogeneous host deposition sites can increase for Na metal, which suppresses Na dendrite formation and alleviates Na metal anode volume undulation [45,46]. Secondly, with the construction of the artificial SEI layer with high mechanical strength and ionic conductivity, it can be tuned to the diffusion kinetics of Na ions, which can avoid the corrosion of the roots of Na metal from the electrolyte and guide the uniform Na metal plating–stripping [47,48]. Thirdly, optimization of the electrolyte formulation, including the design of liquid electrolytes and solid-state electrolytes, can adjust the reactivity of Na metal and improve the migration path of Na ions, which is beneficial to the suppression of Na dendrites [49–53]. In the above method, modifying the Na metal deposition substrate will raise the preparation process and increase the volume of the battery, which restricts the large-scale production of the battery [54]. The process of constructing the artificial SEI layer is equally complicated, and its composition also changes dynamically during the cycle, which eventually makes it unable

to withstand the Na mechanical deformation caused by the growth of Na dendrites [55]. Compared with the first two types of complex processes, electrolyte optimization is simpler and more feasible to improve the electrochemical performance of the Na metal anodes due to the change only in the composition of the electrolytes. Therefore, the optimization of the Na metal anode electrolyte is selected as the main topic in this review.

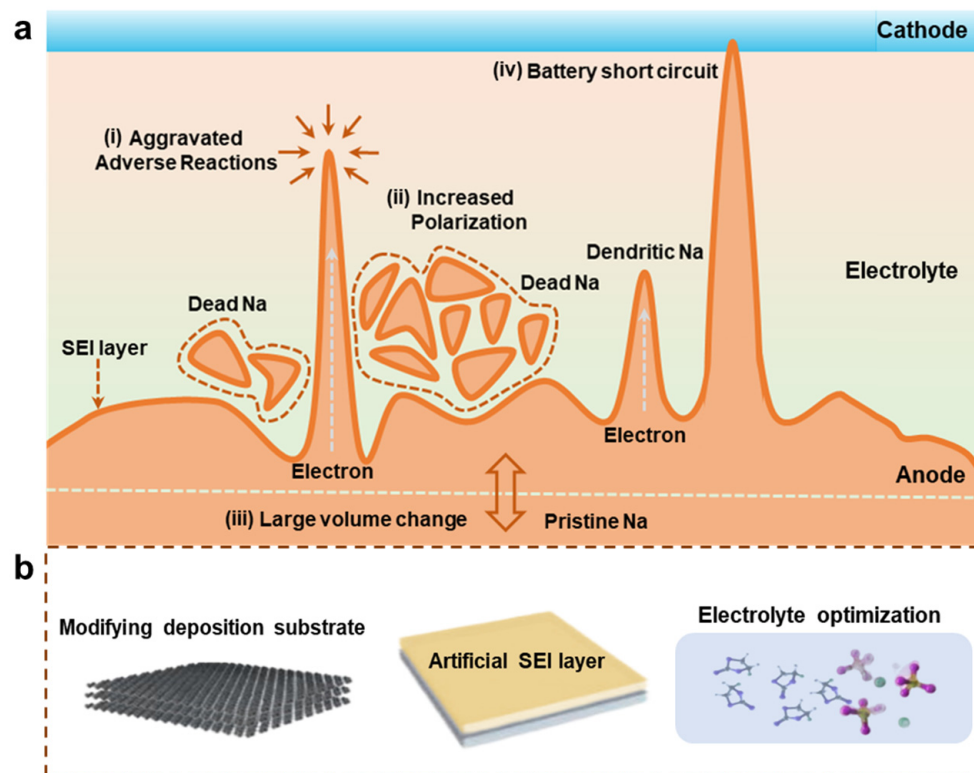


Figure 1. (a) Scheme of dilemmas for the Na metal anode. (b) Three main strategies to resolve the dilemmas for the Na metal anode.

At present, many researchers have reviewed the research progress of Na metal anodes. However, previous progress has focused more on the modification strategy of host materials and artificial SEI layers [56–58]. With the increase in research on electrolyte optimization in the field of Na metal anodes, scientists have found that the method of electrolyte optimization is equally effective and easier to popularize and apply on a large scale. Therefore, it is very necessary to conduct a timely review and summary of some progress in the optimization of electrolytes for Na-metal-based anodes. In this review, we discuss the current Na-metal-based anode electrolytes in three parts: liquid electrolytes, polymer electrolytes, and all-solid-state electrolytes. Firstly, according to the current progress of Na metal anode liquid electrolytes, the effects of electrolyte solvents, solutes, and additives on Na metal anodes are discussed, and their effects on inhibiting Na dendrite growth and improving the electrochemical performance of Na metal anodes are discussed. Secondly, we analyze and discuss the optimization strategies of polymer electrolytes in Na metal anodes and summarize the current progress of polymer electrolytes. In addition, the current preparation method of Na metal anode all-solid-state electrolytes is described to optimize the electrochemical mechanism of Na metal anodes, and the influence of the preparation method of all-solid-state electrolytes on the migration of Na ions is discussed. Finally, we summarize and classify some recent technological advances and research strategies for Na metal anode electrolytes and propose some perspectives and prospects. With the recent increase in the research on Na metal anode electrolytes by scientists, we believe that this review can provide some guidance for the further development of Na metal anode electrolytes.

At present, many researchers have reviewed the research progress of Na metal anodes [57,59]. However, previous progress mainly focused on the modification strategy of host materials and artificial SEI layers [32,60,61]. Although those strategies had some positive effects on the construction of uniform and stable SEI, the complex preparation process made it difficult to popularize on a large scale. With the increase in research on electrolyte optimization for Na metal anodes, scientists found that the method of electrolyte optimization is equally effective and easier to popularize on a large scale [62,63]. Therefore, it is very necessary to conduct a timely review of the progress in the Na metal anode electrolyte optimization. In this review, we mainly discuss the current Na metal anode electrolytes progress in three parts, including liquid electrolytes, polymer electrolytes, and all-solid-state electrolytes. Firstly, we discuss the effects of electrolyte solvents, solutes, and additives in liquid electrolytes for the Na metal anodes and debate how to inhibit the Na dendrite growth and improve the Na metal anode's electrochemical performance. Secondly, we also analyze the optimization strategy of polymer electrolytes in the Na metal anodes and summarize the current progress of polymer electrolytes. Thirdly, the preparation method of Na metal anode all-solid-state electrolytes and expounds on the influence of the electrolyte preparation method for the Na ions migration is described. After the above discussion, we also classify some recent technological advances and research strategies of Na metal anode electrolytes and propose some perspectives. With the recent increase in the research on Na metal anode electrolytes by scientists, we believe that this review can provide some guidance for the further development of Na metal anode electrolytes.

2. Liquid Electrolytes for Na Metal Anodes

The development of Na metal anodes referred to traditional Li metal batteries (LMBs) [50,64]. Therefore, the liquid electrolyte was also applied to the Na metal anodes. However, the conventional LMB electrolyte easily caused the heterogeneous migration and dissolution of Na ions, resulting in the increase in Na dendrites and dead Na. Modification of the electrolyte became necessary. Since 2014, Yoon et al. firstly optimized NaTFSI salt concentrations in N-propyl-nmethylpyrrolidinium bis(fluorosulfonyl)imide ionic liquid to improve the Na metal anodes in the battery [65]. According to the ^{23}Na nuclear magnetic resonance (NMR) spectra, it was found that the chemical shifts and spectral linewidths changed as a function of both salt concentrations, indicating the complex coordination of the Na ion, which was dependent on the salt concentration. The high concentration salt triggered an up-field chemical shift, resulting in the increase in the magnetic shielding. This behavior seemed to facilitate the Na deposition reaction. After the optimization, this high salt concentration in ionic-liquid-based electrolyte presented a stable Na metal plating behavior, with a current of 5 mA cm^{-2} at 25°C to 20 mA cm^{-2} at 100°C . Inspired by this work, many scientists began to devote themselves to the electrolyte engineering research of Na metal batteries (NMBs).

Firstly, it was found that the Na dendrites and dead Na were closely related to the SEI layer, and the SEI layer constituent was partly composed of the decomposition of salts in the electrolyte. Therefore, salt chemistry in electrolyte engineering gained much attention. Seh et al. reported a simple liquid electrolyte, with hexafluorophosphate in glyme (mono-, di-, and tetraglyme) electrolytes for Na metal anodes, which enabled a nondendritic plating-stripping of the Na metal anode with highly reversible performance [62]. They found that NaTFSI salt in the electrolyte caused more exposure of Na metal with the electrolyte solvent, resulting in the trigger of undesirable side reactions. This behavior resulted in the formation of more organic reduction products in the SEI layer and caused a decrease in Coulombic efficiency (CE). Compared with NaTFSI salt, NaPF₆ in electrolyte presented a higher reduction potential than that of glyme solvents, contributing to the formation of a uniform, inorganic SEI layer, which could protect the Na metal surface. Shi et al. introduced potassium bis(trifluoromethylsulfonyl)imide (KTFSI) salt as a bifunctional electrolyte additive [66]. They found that the TFSI⁻ anions in electrolyte assisted in the formation of a stable SEI layer with N-containing species including Na₃N, NaN_xO_y, NaNO₂,

and RNO_2 during the Na plating/stripping process. These N-containing species possessed good Na-ion conductors, which contributed to the mitigation of nonuniform Na dendrite formation. In addition, considering the lower REDOX potential of K/K^+ compared with that of Na/Na^+ , K ions should be adsorbed onto Na protrusions nearby, resulting in the occurrence of electrostatic shielding to suppress Na dendritic deposition. After the optimization, the $\text{Na} \parallel \text{Na}$ symmetric battery in this type of electrolyte presented an average overpotential of 14 mV after cycling for 2700 h. Cao et al. found that highly concentrated ether-based electrolytes exhibited extremely high CEs. The high CEs should be due to the passivation of Na metal surface by the highly concentrated ether-NaFSI mixtures, resulting in the minimizing side degradation reactions during the plating/stripping process [67].

In addition, solvent chemistry was another method used to improve the Na metal anodes. Iermakova et al. compared the performance of Na metal anodes in the electrolytes of 1 M NaPF_6 in both 0.5 ethylene carbonate (EC)/0.5 dimethyl carbonate (DMC) and 1 M NaPF_6 in 0.45 EC/0.45 propylene carbonate (PC)/0.1 DMC ($\text{EC}_{0.45}\text{PC}_{0.45}\text{DMC}_{0.1}$), and found that the $\text{EC}_{0.45}\text{PC}_{0.45}\text{DMC}_{0.1}$ electrolyte presented an enhanced electrochemical performance [68]. However, after immersing the Na metal in the electrolyte for 24 h, large numbers of protrusions were observed on the surface. These limited performance improvements also indicated that carbonate-based electrolytes presented incompatibility for the Na metal anode. To realize the compatibility of the carbonate electrolyte in the Na metal anode, building a stable SEI layer using an electrolyte additive became one of the options. Rodriguez et al. used fluoroethylene carbonate (FEC) as an SEI layer forming additive in a carbonate-based electrolyte for a Na metal anode [69]. They found that the addition of FEC in electrolytes significantly reduced gassing during the deposition process and enhanced the cycling performance. This enhancement performance should be due to the thicker NaF and less dense polymer organic layer in the SEI layer according to the time of flight secondary-ion mass spectrometry (ToF-SIMS) result. Lee et al. also utilized EC/PC solvent with FEC additive and Na bis(fluorosulfonyl)imide (NaFSI) salt as the electrolyte for the Na metal anode [70]. Figure 2a shows the C 1 s, F 1 s, and N 1 s XPS spectra of the Na metal anode surface during the initial Na plating with different electrolytes. They found that the FEC-NaFSI combination electrolyte constructed a homogeneous ionic interlayer during the Na plating/stripping process, containing abundant NaF and ionic compounds, which resulted in the high mechanical strength and ion penetrability of the interlayer. Chen et al. investigated the effects of different cation (Li^+ , K^+ , Mg^{2+} , Ca^{2+} , Cu^{2+} , Zn^{2+} , and Al^{3+}) additives on electrolyte stability and the corresponding electrolyte solvation structures according to DFT calculation, as shown in Figure 2b [71]. Due to the lower electrode potential than Na-metal anodes, Li^+ , K^+ , and Ca^{2+} are suggested as cation additives. In addition, considering the LUMO level and the binding energy, Li^+ is expected to be the most outstanding candidate. Therefore, they attempted to introduce Li^+ additives into the 1 M NaPF_6 -DME electrolyte for NMBs. From the in situ optical microscopic characterizations, it was observed that the Na metal deposit exhibited a needle-like shape after deposition in 1 M NaPF_6 -DME electrolyte. After the introduction of Li^+ additives, the Na metal showed a smooth morphology deposition, which was extremely disparaged from the needle-like Na dendrites. This result validated the resisted Na dendritic growth due to the electrostatic shield effect and enhanced electrolyte stability after introducing Li^+ additives.

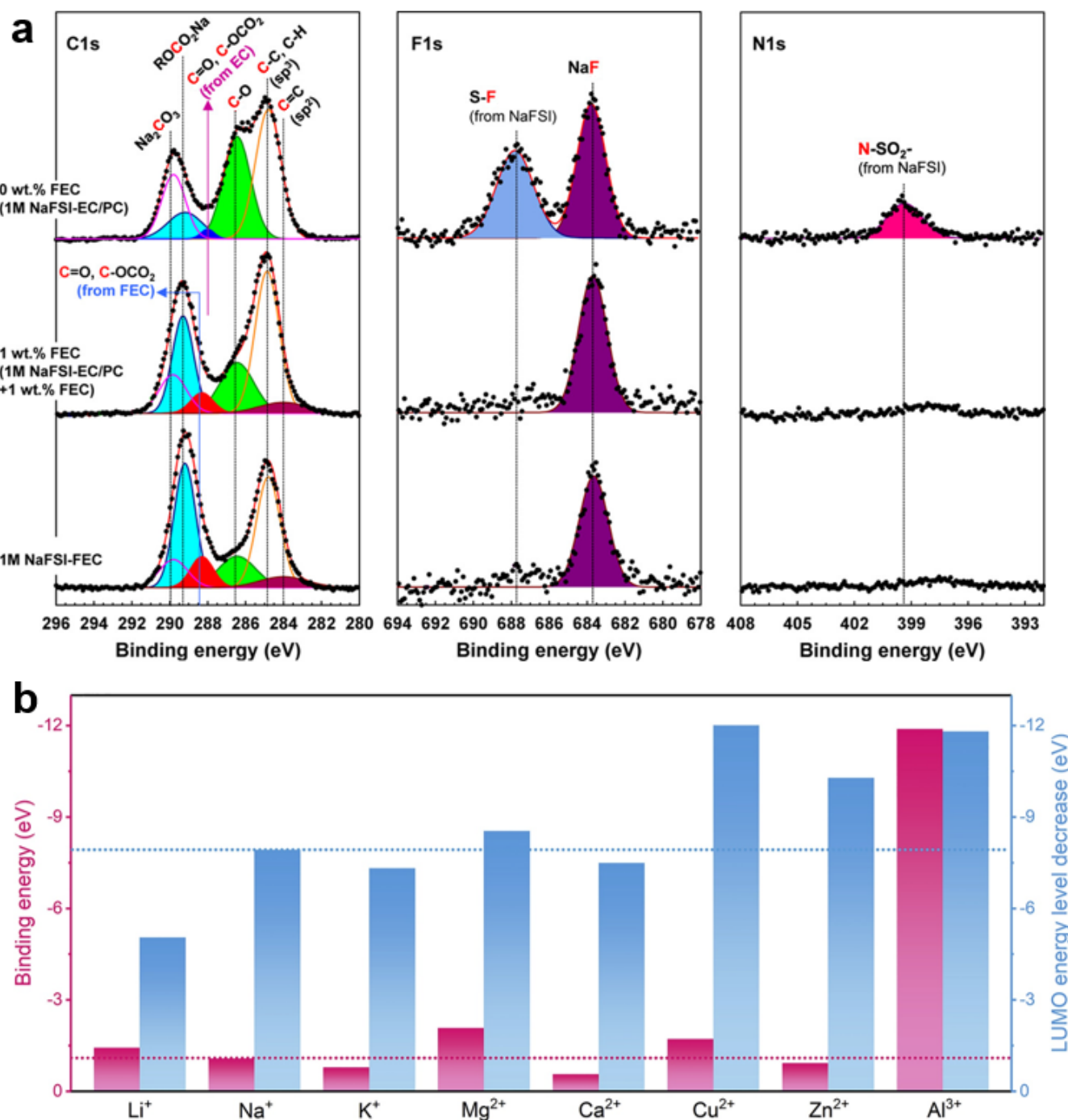


Figure 2. (a) C 1 s, F 1 s, and N 1 s XPS spectra of the Na metal anode surface during the initial Na plating. Reproduced with permission from Reference [70] Copyright 2018, American Chemical Society. (b) The comparison of LUMO energy levels decreases and binding energy of ion–DME complexes. Reproduced with permission from Reference [71] Copyright 2020, Elsevier.

From the aforementioned discussion, it is found that the increase in inorganic constituents, especially NaF could improve the stability of the SEI layer, leading to the electrochemical enhancement performance for NMBs. Based on this result, the F-containing ingredients were also utilized as electrolyte additives in NMBs. Fang et al. utilized SbF_3 as an electrolyte additive in 4 M NaFSI-DME-based electrolytes for NMBs and found that the SbF_3 additive could build a bilayer SEI layer [72]. One layer was constituted by the Na-Sb alloy layer from the Sb-ion electrolyte. Another layer was derived from the F ion of the SbF_3

additive, resulting in the formation of the NaF-rich SEI layer on the Na metal surface, as shown in Figure 3a. Due to these features of the bilayer SEI layer, the Na || Na symmetric battery presented enhanced stable cycling of 1000 h at the current density of 0.5 mA cm^{-2} . Not only the F-containing ingredient but some other additives also contributed to the increase in the high F-containing substance in the SEI layer for NMBs. Fang et al. designed a localized high-concentration electrolyte (LHCE) with an SbF₃ electrolyte additive as NMB's electrolyte [51]. They found that the SbF₃ electrolyte additive would create a stabilized SEI layer with a Na–Sb alloy inner layer and a NaF-rich outer layer, which could protect the Na metal anode. As expected, the Na || Na symmetric battery in this type of electrolyte presented a long cycle life of over 1200 h at 0.5 mA cm^{-2} with negligible voltage polarization. Jiang et al. found that the acetamide (N, O-bis(trimethylsilyl) trifluoroacetamide, BSTFA) additive acted as a scavenger, scavenging the HF and H₂O, which restrained the hydrolysis reaction in the NaPF₆ in the electrolyte [73]. These behaviors were also in favor of the high F-containing substance in the SEI layer. After the introduction of BSTFA into ultralow-concentration electrolytes with 0.3 M NaPF₆, the Na metal anode still presented a high-capacity retention rate of 92.63% after 1955 cycles at 2 C.

In stabilizing the SEI layer to achieve Na metal anode stability, some new ideas were to improve the stability of NMBs from the perspective of solvation. Firstly, Doi et al. designed a concept of F-free electrolytes, 0.1 M Na tetraphenylborate (NaBPh₄) in DME for NMBs. They found that the F-free electrolyte enabled a high reversible Na plating/stripping at the average Coulombic efficiency of 99.85% over 300 cycles. Due to the F-free design of the electrolyte, the SEI layer onto the Na metal anode was mainly composed of the C, O, and Na elements with the negligible presence of the F element. After cycling for 450 h, the Na || Na symmetric battery only presented the interphase resistance of 3Ω in NaBPh₄/DME electrolyte, indicating that extremely stable and low-resistivity interphase was formed. Figure 3b showed the DC-DFTB-metaD simulations, which could be used to evaluate the two-dimensional free energy surface concerning various coordination states. From this simulation, they found that the most stable state of [BPh₄]⁻ in NaBPh₄/DME was CIP after the fully dissociated state. This result also indicated that [BPh₄]⁻ was the most tolerant against the reduction, which accounted for the stable Na/electrolyte interphase. In addition, the other substances also could be used to improve the stability of the NMBs. Zheng et al. attempted to add a small amount of SnCl₂ into carbonate electrolyte for NMBs and found that the Na || Na symmetric battery achieved a remarkable reduction of voltage hysteresis for over 500 h [74]. To investigate the reasons for this performance improvement, they took the symmetric battery apart for characteristics. They found that SnCl₂ in electrolytes could spontaneously react with Na metal to form a Na-Sn alloy layer due to the hyper-reductivity of Na metal. In addition, the Cl⁻ also reacted with Na metal to produce a NaCl-rich SEI, which could passivate Na metal surface against the corrosion from electrolyte during the plating–striping process. Figure 3c showed the schematic of the typical mosaic SEI on the Na metal anode in the regular carbonate electrolyte and SnCl₂-containing carbonate electrolyte. Kreissl et al. introduced a functionalized diamondoid (bis-N,N'-propyl-4,9-dicarboxamidediamantane, DCAD) as an electrolyte additive for NMBs [75]. They found that the functionalized diamantine additive could change the SEI constituent as well as the co-deposition behavior of Na ions, resulting in the change in Na metal growth direction in the plated Na process. Wang et al. found that the slight Na polysulfide (Na₂S₆) served as an electrolyte additive, which could pre-passivate the Na metal anode in ether electrolyte [76]. According to the interface analysis, the slight Na polysulfide introduction resulted in the robust SEI layer composed of Na₂O, Na₂S₂, and Na₂S, which could protect the Na metal against damage from electrolyte components. It is generally believed that the NaNO₃ additives in the electrolyte can protect electrodes and inhibit dendrite formation in LMB. However, a strange phenomenon was that the co-additive of Na₂S₆-NaNO₃ presented seriously deteriorated the Na metal electrode, with an adverse effect for NMBs, which was contrary to the LMBs. Zhu et al. developed an organosulfur compound (tetramethylthiuram disulfide, TMTD) as an additive in carbonate-

based electrolytes to enhance the electrochemical performance of the Na metal anode [63]. They found that TMTD could *in situ* generate a stable SEI layer as an interfacial protection layer on the Na metal surface. According to the constituent analysis, the SEI layer was constituted by the rich organic sulfide salts, which could be more conducive to maintaining the stability of the Na metal anode during the stripping/plating process. In addition, it was found that a very high CE of 94.25% could be delivered and the full battery also achieved a high reversible capacity of 86.2 mAh g^{-1} after 600 cycles at 4 C.

For the Na metal anodes, Na dendrite growth would lead to separator puncture, which triggered the combustion events of the battery. Therefore, the exploitation of non-inflammable electrolytes also was a pursuit direction for NMBs. Yi et al. designed a low-flammable electrolyte, which consisted of 1 M NaPF_6 in DME, FEC, and 1,1,1,3,3,3-hexafluoroisopropylmethyl ether (HFP) with a volume ratio of 2:1:2 (denoted as NaPF_6 -FRE) for NMBs [77]. They found that $\text{Na} \parallel \text{Na}$ symmetric battery in NaPF_6 -FRE electrolyte exhibited a superior cycling performance for 800 h with a stable voltage profile (1 mA cm^{-2} , 1 mAh cm^{-2}), which was much higher than that of the $\text{Na} \parallel \text{Na}$ symmetric battery in electrolyte without an HFP (1 M NaPF_6 in DME/FEC) electrolyte. They suggested that the addition of HFP would generate a new F-containing SEI layer, which could stabilize the Na metal surface. In addition, the NaPF_6 -FRE electrolyte also presented a wide electrochemical window of 5.2 V. Zheng et al. utilized superior miscibility of all-fluoride fire extinguishant into fluorinated carbonate electrolytes (N-FEPH + P) for NMBs [78]. Considering the addition of an all-fluoride fire extinguishant in the electrolyte, the flaming fire was also quenched in the N-FEPH-P electrolyte. With the all-fluoride fire extinguishant, the $\text{Na} \parallel \text{Na}$ symmetric battery performance in the N-FEPH + P electrolyte could greatly improve. The cycle of 1100 h at 1.0 mAh cm^{-2} and 800 h at 5.0 mAh cm^{-2} could be received in $\text{Na} \parallel \text{Na}$ symmetric battery with N-FEPH + P electrolyte. After matching the $\text{Na}_3\text{V}_2(\text{PO}_4)_2\text{O}_2\text{F}$ cathode, the full battery also presented a high initial CE of 94.7% and capacity retention of 87.1% after 1000 cycles at 0.5 C. After disassembling the battery, they found that a thin F-rich SEI layer was established on both the Na metal anode and the cathode in the N-FEPH + P electrolyte, which facilitated the efficient Na metal plating/stripping and enhanced the cycle life of over 1000 cycles in full batteries. As one low dielectric constant and highly fluorinated and intrinsically nonflammable ether, 1,1,2,2-tetra-fluoroethyl 2,2,3,3-tetrafluoropropyl ether (HFE) and trimethyl phosphate (TMP) were also considered for used in electrolyte for NMBs. Liu et al. introduced two functional fluorinated solvents of HFE and FEC into the TMP-based electrolyte for NMBs [79]. Under the flame burning, the electrolyte-soaked separator still had not ignited, indicating that this type of TMP-FEC-HFE-based electrolyte was fire resistant. For NMBs, the $\text{Na} \parallel \text{Na}$ symmetric battery presented the cycle for 800 h at 1.0 mA cm^{-2} or 3.0 mAh cm^{-2} . They also suggested that the non-solvating HFE plays a critical role in local electrolyte concentration to decrease the unfavorable decomposition of TMP.

From the aforementioned discussion, we also summarized the important parameters, including electrolyte constituents, cycling stability, and full battery performance of liquid electrolyte recently reported NMBs in Table 1.

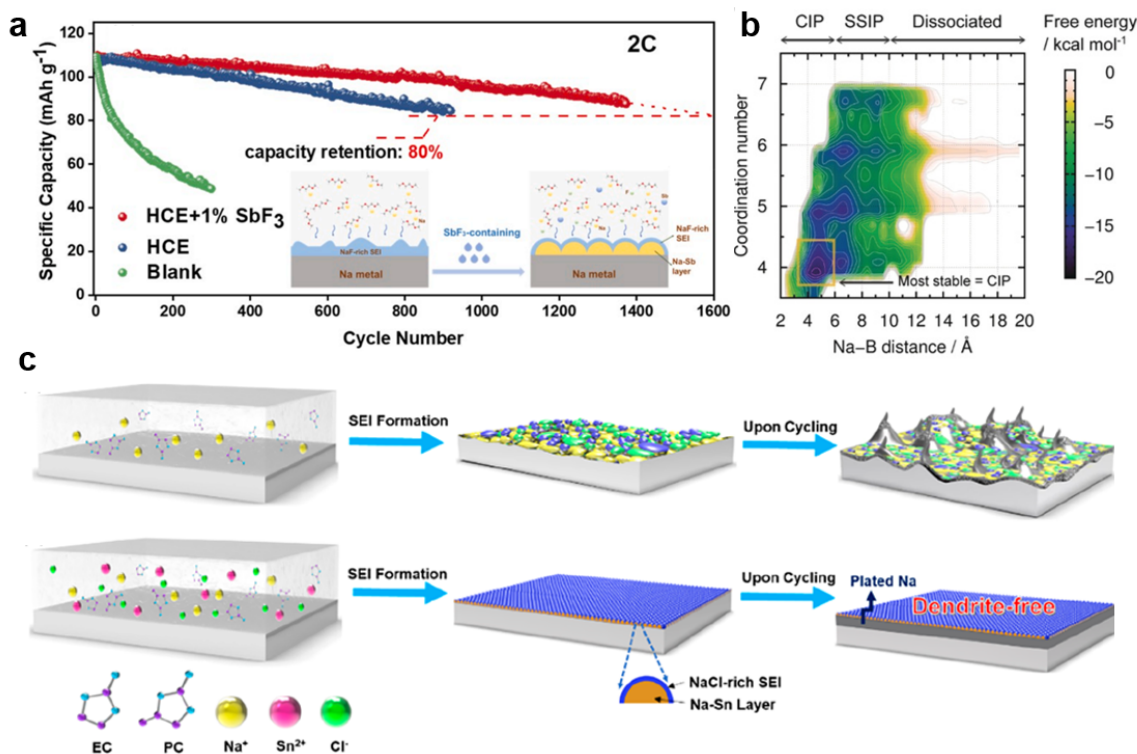


Figure 3. (a) Cycling performance. Voltage profiles of the $\text{Na} \parallel \text{NVP}$ battery tested at 2 C after different cycle numbers using HCE + 1% SbF_3 , HCE, and blank electrolyte, the inset is the formation mechanism illustration of a typical SEI layer on the Na metal anode using HCE + 1% SbF_3 electrolytes. Reproduced with permission from Reference [72] Copyright 2020, Elsevier. (b) Two-dimensional free energy surface for the ion-pair distance and coordination number between Na and DME of $\text{NaBPh}_4/\text{DME}$ solution, reproduced with permission from Reference [80] Copyright 2019, Wiley–VCH. (c) Schematics of the typical mosaic SEI on the Na metal anode cycled in regular carbonate electrolyte and the in situ formed Na-Sn alloy layer plus a NaCl-rich SEI layer. Reproduced with permission from Reference [74] Copyright 2019, American Chemical Society.

Table 1. Electrochemical properties of different liquid electrolytes in NMBs.

Liquid Electrolytes	Symmetrical Cell (Cycle Performance (h)@Current Density (mA cm^{-2}))	CE ([ICE@Cycle Number@Current Density (mA cm^{-2}))	Full Cell (Cathode@Capacity (mAh g^{-1})@Current Density (C))	References
1 M NaPF_6 in diglyme	/	99.9%@300@0.5	S@776@0.1	[62]
NaFSI/DME (1:2 v/v)	200@0.2	97.7%@250@0.2	91% 100 cycles	[81]
0.5 M $\text{NaBF}_4/\text{G2}$	3000@0.5	99.93%@400@0.5	$\text{Na}_3\text{V}_2(\text{PO}_4)_3$ @100@0.1	[82]
1 M $\text{NaBF}_4/\text{TEGDME}$	1000h@0.2	99.9%@1000@0.5	P2- $\text{Na}_{2/3}\text{Co}_{1/3}\text{Mn}_{2/3}\text{O}_2$ @163@0.1	[83]
1 M $\text{NaPF}_6/\text{TEGDME}$	1000@0.2	99.9%@850@0.5	P2- $\text{Na}_{2/3}\text{Co}_{1/3}\text{Mn}_{2/3}\text{O}_2$ @172@0.1	[83]
1 M NaFSI/FEC	100@5.56	94%@100@0.28	/	[70]
0.1 M $\text{NaBPh}_4/\text{DME}$	500@0.5	99.85%@300@0.5	/	[80]
1 M $\text{NaClO}_4/\text{EC}/\text{PC} + 5 \text{ wt\% FEC}$	100@1	88%@50@1	/	[84]
1 M $\text{NaPF}_6/\text{DME}/\text{FEC}/\text{HFPF}$ (2:2:1 v/v)	800@0.5	99%@2000@5	$\text{Na}_3\text{V}_2(\text{PO}_4)_3$ @89.1@0.5	[77]
1 M NaPF_6 in diglyme + 0.033 M Na_2S_6	400@2	99%@500@0.5	S@621@1	[76]
1 M NaTFSI/FEC + 0.75% NaAsF_6	350@0.5	97%@400@0.1	$\text{Na}_3\text{V}_2(\text{PO}_4)_3$ @~102@1	[85]
1 M $\text{NaClO}_4/\text{EC}/\text{PC} + 50 \text{ mM SnCl}_2$	500@0.5	/	$\text{Na}_3\text{V}_2(\text{PO}_4)_3$ @101@10	[74]
2 M NaFSI/DME/FEPE(1:1 molar ratio) + 1% SbF_3	1200@0.5	99%@20@1	$\text{Na}_3\text{V}_2(\text{PO}_4)_3$ @105@10	[51]
1 M $\text{NaClO}_4/\text{EC}/\text{PC} + 1\% \text{SbF}_3$	1000@0.5	/	$\text{Na}_3\text{V}_2(\text{PO}_4)_3$ @80@40	[72]
0.8 M $\text{LiPF}_6/\text{DME} + 1 \text{ M NaPF}_6/\text{DME}$	150@0.5	99.2%@100@0.2	LiFePO_4 @62.4@20	[34]
1 M NaOTf/DME + 0.01 M KTFSI	2700@1	99.5%@300@0.5	/	[66]
1 M $\text{NaClO}_4/\text{EC}/\text{PC} + 0.5 \text{ mM C}_6\text{(NO}_2\text{)}_6$	500@0.5	99.4%@200@5	$\text{Na}_3\text{V}_2(\text{PO}_4)_3/\text{C}$ @95.9@5	[86]

Table 1. Cont.

Liquid Electrolytes	Symmetrical Cell (Cycle Performance (h)@Current Density (mA cm ⁻²))	CE (ICE@Cycle Number@Current Density (mA cm ⁻²))	Full Cell (Cathode@Capacity (mAh g ⁻¹)@Current Density (C))	References
1 M NaPF ₆ /DME + 0.1 wt% C ₆₀ (CF ₃) ₆	1200@2	99.6%@780@1	Na ₃ V ₂ (PO ₄) ₃ /C@108@10	[87]
1 M NaPF ₆ /EC/PC + 2 wt% TMTD	1600@0.25	/	Prussian blue@70@10	[63]
1 M NaPF ₆ in diglyme + 5 mM CTAB	500@3	/	C/S@640@0.5	[88]
1 M NaPF ₆ /FEC/PC/HFE + PFMP	1100@0.5	94.2%@100@0.5	Na ₃ V ₂ (PO ₄) ₂ O ₂ F@113@2	[78]
0.3 M NaPF ₆ /EC/PC + 2 wt% BSTFA	350@0.5	/	Na ₃ V ₂ (PO ₄) ₃ @105@40	[73]
0.8 M NaPF ₆ /TEP/FEC + 5 wt% DTD	1300@0.5	93.4%@250@0.5	Prussian blue@78.8@10	[89]
4 M NaFSI/DME	/	99%@300@0.5	Na ₃ V ₂ (PO ₄) ₃ @-100@0.2	[67]
5 M NaFSI/DME	600@0.0028	99.3%@120@0.056	Na ₄ Fe ₃ (PO ₄) ₂ (P ₂ O ₇)@109.4@0.5	[90]
2.1 M NaFSI/DME/BTFE(1:2 v/v)	950@2	98.98%@400@1	Na ₃ V ₂ (PO ₄) ₃ @92@10	[91]
2 M NaFSI/DME/TTE	1170@0.2	/	Na ₃ V ₂ (PO ₄) ₃ @101.5@40	[50]

3. Polymer Electrolytes for Na Metal Anodes

In the Na metal anodes, the non-uniform Na metal deposition results in the formation of Na dendrite. With the continuous growth of Na dendrites, the separator eventually was pierced, which led to the short circuit of the NIBs and caused serious safety hazards. The previous liquid electrolyte optimization could effectively inhibit the growth of the Na dendrite. However, it was still difficult to ensure the inhibition of the Na dendrite in the manufacturing process. To prevent the piercing of the Na dendrite triggering the short circuit in NMBs, developing solid-state NMBs became a candidate species due to the high thermal stability of inorganic solid-state electrolytes and the toleration of higher potential. Additionally, due to the reduction of liquid electrolytes, the packaging for solid-state NMBs would be simplified, resulting in a decrease in dead weight in battery packaging.

In solid-state electrolytes, polymer electrolytes were the most common choice [92–95]. Inspiring the polymer electrolytes from the Li metal anode, several polymer electrolytes were designed for the Na metal anode. Zheng et al. firstly developed Na-containing hybrid network solid polymer electrolytes (SPEs) for NMBs [96]. The SPEs were synthesized by crosslinking of octakis(3-glycidyloxypropyltrimethylsiloxy) octasilsesquioxane and amine-terminated polyethylene glycol with NaClO₄ (POSS-4PEG2K). Figure 4a shows a photograph of a hybrid crosslinked SPE membrane and the transparent and easy handle of the membrane could be observed. After optimization, they found that this type of polymer electrolyte exhibited a high conductivity of 0.256 mS cm⁻¹ at 80 °C. As the solid-state electrolyte for Na metal anodes, they found that the Na|Na symmetric battery presented the cycling performance of 5150 and 3550 h at 0.1 and 0.5 mA cm⁻², respectively. Wang et al. prepared a single ion conducting gel polymer electrolyte (PSP-GPE) for NMBs, which presented an excellent ionic conductivity of 0.1 mS cm⁻¹ and a high Na-ion transference number of 0.88 at room temperature (RT), which was close to the NaClO₄-based liquid electrolyte [97]. When the Na₃V₂(PO₄)₃ cathode was coupled with PSP-GPE, the full battery exhibited an improvement in cycling performance and the Na dendrites could be effectively restrained. Sangeland et al. utilized poly(trimethylene carbonate) (PTMC) as a host material for NMB's electrolyte and used NaFSI as the Na salt to obtain the polymer electrolyte (PTMC-NaFSI) [98]. Through the optimization of the Na salt concentration, they found that the carbonate: Na⁺ ratio of 1:1 in polymer electrolyte presented the highest ionic conductivity of 50 μS cm⁻¹ at 25 °C, and the carbonate: Na⁺ ratio of 5:1 exhibited a more stable capacity of about 90 mAh g⁻¹ over 80 cycles at 60 °C in the Na metal full battery with a Prussian blue cathode. Wen et al. reported an ethoxylated trimethylolpropane triacrylate-based polymer electrolyte (ETPTA-NaClO₄-QSSE) using photopolymerization for NMBs [99]. Figure 4b shows the optical images of ETPTA-NaClO₄-QSSE before and after UV curing and found the ETPTA-NaClO₄-QSSE would be solidified after UV curing. From the ionic conductivity of ETPTA-NaClO₄-QSSE during varying temperature in Figure 4c, the ionic conductivity 0.7, 0.8, 1.0, 1.2, 1.4, 1.5, and 1.8 mS cm⁻¹ could be received at -10, 0, 15, 25, 40, 60, and 80 °C, respectively. These results indicated that ETPTA-NaClO₄-QSSE presented excellent temperature adaptability. As the polymer electrolyte

in NMBs, the $\text{Na} \parallel \text{Na}$ symmetrical battery presented very low overpotential of about 70 mV and retained an ultra-stable cycling performance for 1000 h (Figure 4d). Zhang et al. utilized a Cu-based metal-organic framework (MOF) to support the poly(ethylene oxide) (PEO) with NaClO_4 under UV curing as polymer electrolyte (PEO-Cu-MOF) [100]. After solidification, the Cu-based MOF was uniformly dispersed into the PEO matrix. Owing to the high specific surface areas and ordered porous structures of Cu-based MOF, the PEO-Cu-MOF polymer electrolyte exhibited a high ionic conductivity of 3.48 mS cm^{-1} . Figure 4e shows the cycling performance of the $\text{Na} \parallel \text{Na}$ symmetrical battery with the PEO-Cu-MOF polymer electrolyte at different current densities and capacities. A very stable polarization voltage also could be observed, indicating the excellent interfacial stability between the electrolyte and electrode.

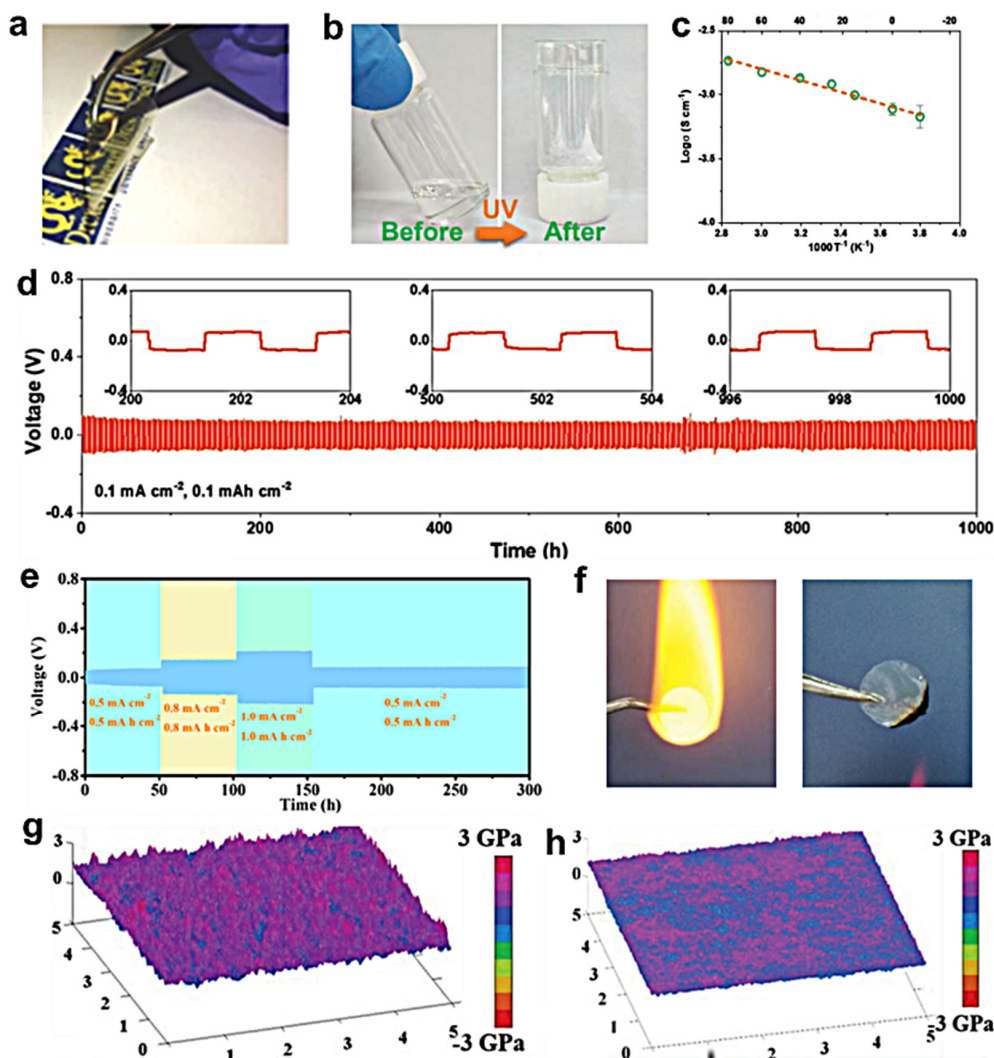


Figure 4. (a) Photograph of a hybrid crosslinked SPE membrane, reproduced with permission from Reference [96] Copyright 2018, Wiley–VCH. (b) Photograph of ETPTA- NaClO_4 -QSSE before and after UV curing. (c) Ionic conductivity of ETPTA- NaClO_4 -QSSE under varying temperatures. (d) Cycling profiles of the symmetrical battery at 0.1 mA cm^{-2} for 1 h, reproduced with permission from Reference [99] Copyright 2021, Wiley–VCH. (e) Cycling profiles of the symmetric battery at different current densities, reproduced with permission from Reference [100] Copyright 2021, American Chemical Society. (f) Flame test of glass fiber saturated with $1.0 \text{ M NaClO}_4/\text{PC}$ and P(MVE-alt-MA), reproduced with permission from Reference [101] Copyright 2019, Springer Nature. Surface Young's modulus of (g) 2-GPH and (h) PH, reproduced with permission from Reference [102] Copyright 2020, Wiley–VCH.

In addition, some functional polymer solid-state electrolytes were also being investigated. Yang et al. used poly(methyl vinyl ether-alt-maleic anhydride) (P(MVE-alt-MA)) as the polymer host, bacterial cellulose (BC) as the reinforcement, and triethyl phosphate (TEP)/vinylene carbonate (VC)/NaClO₄) as a plasticizer to obtain the polymer electrolyte (BC-TEP/VC/NaClO₄) for NMBs [101]. They found that polymer electrolyte presented flame retardancy due to the addition of TEP (Figure 4f). In addition, an electrochemical window of 4.4 V could also be received. As the polymer electrolyte for NMBs, Na₃V₂(PO₄)₃/Na full batteries exhibited an 84.4% capacity retention after 1000 cycles, which was much better than that of the full battery in the liquid electrolyte. Furthermore, the polymer electrolyte also provided an 84.8% capacity retention after 50 cycles at −10 °C in Na₃V₂(PO₄)₃/Na full batteries. Luo et al. developed a polymer electrolyte constituted by graphene oxide (GO) and PVDF-HFP with a high mechanical property and found that the 2 wt%GO-PVDF-HFP presented the highest Young's modulus of 2.5 GPa and high ionic conductivity of 2.3 mS cm^{−1} (Figure 4g,h) [102]. The high mechanical property of polymer electrolytes could suppress the Na dendrite growth and avoid puncture by the Na dendrite. As result, the Na||Na symmetric battery in 2 wt%GO-PVDF-HFP electrolyte exhibited an ultra-long cycling performance over 400 h at 5 mA cm^{−2}.

Solid-state Na-O₂ batteries had been regarded as promising energy storage devices due to their high energy density, ultralow overpotential, and abundant resources. Chen et al. reported a quasi-solid-state polymer electrolyte (QPE) composed of poly(vinylidene fluoride-co-hexafluoropropylene)-4% SiO₂-NaClO₄-tetraethylene glycol dimethyl ether (TEGDME) for high-performance Na-O₂ batteries [103]. The abundant fluorocarbon chains of QPE played an important role in Na⁺-ion transfer, resulting in a high ionic conductivity of 1.0 mS cm^{−1}. The Na-O₂ batteries exhibited negligible voltage decay after cycling for 80 cycles at a cutoff discharge capacity of 1000 mAh g^{−1}.

After the aforementioned discussion, we also summarized the important parameters, including electrolyte constituents, cycling stability, and full battery performance of polymer electrolyte recently reported NMBs in Table 2.

Table 2. Electrochemical properties of different polymer electrolytes in NMBs.

Polymer Electrolytes	Ionic Conductivity (mS cm ^{−1})@Temperature (°C)	Symmetrical Cell (Cycle Performance (h)@Current Density (mA cm ^{−2}))	Full Cell (Cathode@Capacity (mAh g ^{−1})@Current Density (C))	References
POSS-4PEG2K	4.5 × 10 ^{−3} @30	3550@0.5	Na _x V ₂ O ₅ @305@0.05	[96]
PSP-GPE	0.1@RT	620@1	Na ₃ V ₂ (PO ₄) ₃ @89.1@0.2	[97]
PTMC-NaFSI	0.05@25	/	Prussian blue@90@0.2	[98]
ETPTA-NaClO ₄ -QSSE	1.2@RT	1000@0.1	Na ₃ V ₂ (PO ₄) ₃ @101@1	[99]
PEO-Cu-MOF	3.48@RT	1000@0.2	NaCrO ₂ @120.7@0.1	[100]
IL-MOF	0.36@RT	500@1	Na ₃ Ni _{1.5} TeO ₆ @83.8@0.1	[104]
BC-TEP/VC/NaClO ₄	0.22@RT	/	Na ₃ V ₂ (PO ₄) ₃ @84.3@0.2	[101]
GO-PVDF-HFP	2.3@RT	400@5	Na ₃ V ₂ (PO ₄) ₃ @107@1	[102]
NaPTAB-SGPE	0.094@RT	100@0.05	Na ₃ V ₂ (PO ₄) ₃ @90.3@0.05	[105]
SILGM	2@23	/	Na ₃ V ₂ (PO ₄) ₃ @81.7@0.1	[106]

4. All-Solid-State Electrolytes for Na Metal Anodes

Except for polymer electrolytes, the scientists also were looking at the all-solid-state electrolytes for NMBs. As the all-solid-state electrolytes in NMBs, several essential requirements needed to be met: (1) possessing high ionic conductivity of above 10^{−4} S cm^{−1} at RT; (2) possessing a high ionic transference number; (3) possessing negligible conductivity; and (4) possessing a wide electrochemical window. Based on these essential requirements, the scientists set out to develop all-solid-state electrolytes for NMBs.

Borrowed from a Li metal all-solid-state electrolyte, Na-β"-Al₂O₃ first received research attention from scientists [107–109]. Wen et al. explored the viability and stability of Na₃PS₄ and Na-β"-Al₂O₃ for NMBs [110]. They found that the Na₃PS₄ and Na-β"-Al₂O₃

presented conductivities of 2.1 and 0.04 mS cm^{-1} , respectively. The Nyquist plots of Na_3PS_4 and $\text{Na}-\beta''-\text{Al}_2\text{O}_3$ electrolyte for the fresh contact and after 12 h of contact in NMBs were also compared. They found that Na_3PS_4 presented an increased impedance after 12 h of contact. Compared with Na_3PS_4 , $\text{Na}-\beta''-\text{Al}_2\text{O}_3$ exhibited almost no change over time, indicating that $\text{Na}-\beta''-\text{Al}_2\text{O}_3$ presented stability against the reaction with the Na metal anode. Considering the high interface resistance in the $\text{Na}-\beta''-\text{Al}_2\text{O}_3$ electrolyte, modification of this electrolyte to reduce the interfacial resistance became the direction of efforts. Wu et al. attempted to create an $\text{Na}-\beta''-\text{Al}_2\text{O}_3$ electrolyte for NMBs with the introduction of the coating layer, which was constituted by cotton-cloth-derived disordered carbon tubes (DCTs) [111]. The corresponding solid-state electrolyte was denoted as BASE-CNT. They found that $\text{Na}-\beta''-\text{Al}_2\text{O}_3$ electrolyte presented a great decrease in interfacial resistance from 750Ω to $150 \Omega \text{ cm}^{-2}$ after DCT modification. Therefore, the modified $\text{Na}-\beta''-\text{Al}_2\text{O}_3$ electrolyte exhibited stable Na stripping–plating profiles of 400 cycles at 0.1 mA cm^2 with a small hysteresis of 100 mV. Deng et al. developed yttria-stabilized zirconia (YSZ) to enhance the $\text{Na}-\beta''-\text{Al}_2\text{O}_3$ electrolyte for NMBs and found that the YSZ introduction on the surface of the $\text{Na}-\beta''-\text{Al}_2\text{O}_3$ electrolyte could extremely reduce the interface impedance of $3.6 \Omega \text{ cm}^{-2}$ at 80°C and presented a high critical current density of 7.0 mA cm^{-2} [112]. From the surface and cross-section SEM images of the YSZ-Na- $\beta''-\text{Al}_2\text{O}_3$, it was found that YSZ particles (white) were homogeneously distributed in $\text{Na}-\beta''-\text{Al}_2\text{O}_3$. Figure 5a showed a Swagelok-type battery schematic to investigate the interfacial stability of YSZ-Na- $\beta''-\text{Al}_2\text{O}_3$ solid-state electrolyte in a symmetric battery. From the EIS profiles in Figure 5b, the YSZ-Na- $\beta''-\text{Al}_2\text{O}_3/\text{Na}$ interfacial areal specific resistance was $18.8 \Omega \text{ cm}^2$ at RT and $3.6 \Omega \text{ cm}^2$ at 80°C after removing the contributions from the bulk and grain boundary. Due to the low interfacial areal specific resistance, $\text{Na} \parallel \text{Na}$ symmetric battery with YSZ-Na- $\beta''-\text{Al}_2\text{O}_3$ solid-state electrolyte presented a small cell voltage (<50 mV) even at a high areal capacity of 2.5 mAh cm^{-2} (Figure 5c). From the SEM images of the YSZ-Na- $\beta''-\text{Al}_2\text{O}_3$ solid-state electrolyte cycling at different times at 80°C in Figure 5d–g, intimate contact between the electrolyte and Na metal anode still could be observed, which contributed to the Na-ion transfer from the electrolyte to the Na metal anode. Chi et al. also developed a solid-state electrolyte of $\beta''-\text{Al}_2\text{O}_3$ with a nano Sn interlayer, denoted as Sn-BASE, and used an organic quinone-based compound (pyrene-4,5,9,10-tetraone, PTO) as the cathode for NMBs [113]. They found that this Sn-BASE-PTO electrolyte allowed the $\text{Na} \parallel \text{Na}$ symmetric battery presenting a high stability of 1000 h at 0.5 mA cm^{-2} . In addition, after Sn thin film introduction, the interfacial resistance between the Na metal anode and the electrolyte could be reduced to $26.7 \Omega \text{ cm}^{-2}$. Furthermore, they suggested that the mechanically compliant PTO-based composite would form an interpenetrating ionic and electronic pathway, which contributed to overcoming the cathode–electrolyte interfacial barrier.

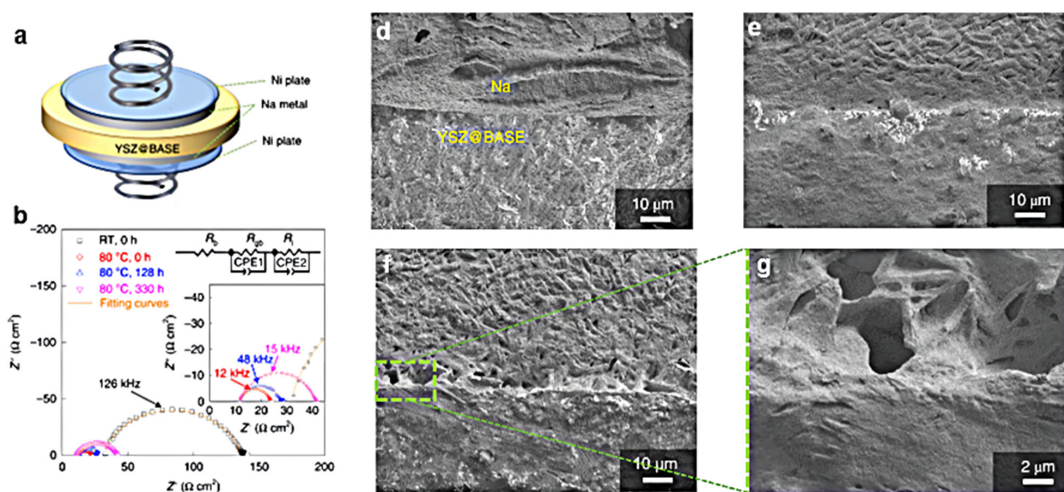


Figure 5. Cont.

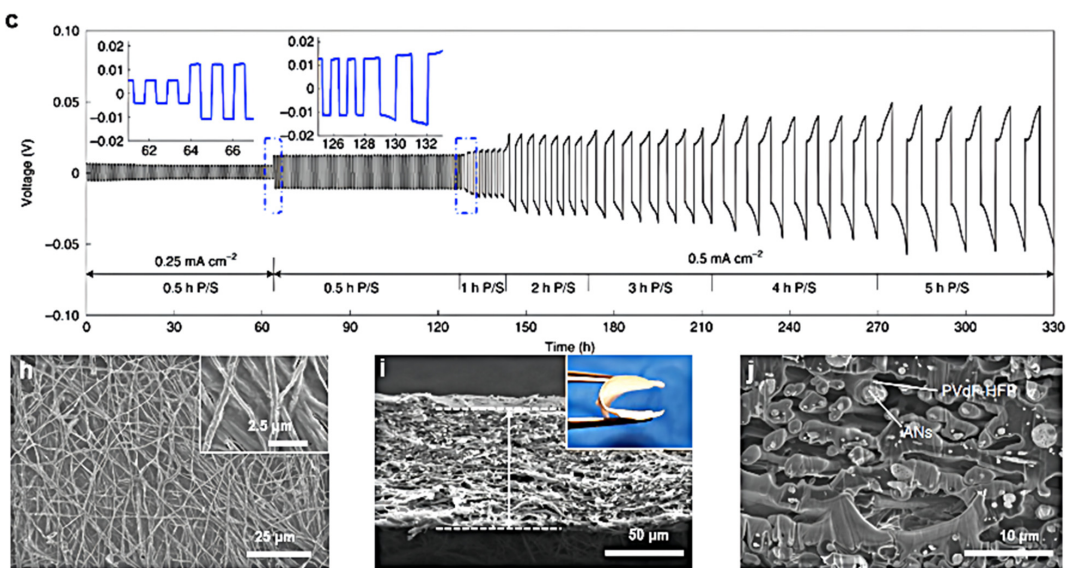


Figure 5. (a) Schematic configuration of $\text{Na} \parallel \text{Na}$ symmetric battery; (b) comparison of EIS of the Na symmetric cells at RT and $80\text{ }^{\circ}\text{C}$ with the cycling of 0, 128, and 330 h; (c) galvanostatic cycling of the Na symmetric cell at $80\text{ }^{\circ}\text{C}$ at 0.25 and 0.50 mA cm^{-2} ; the corresponding SEM images of $\text{YSZ-Na-}\beta''\text{-Al}_2\text{O}_3/\text{Na}$ interfaces at $80\text{ }^{\circ}\text{C}$ with cycling times of (d) 0 h, (e) 128 h, and (f,g) 330 h, reproduced with permission from Reference [112] Copyright 2022, Springer Nature. (h) Surface, (i) cross-sectional SEM images, and (j) enlarged cross-sectional SEM image of ANs-PVDF-HFP membranes, reproduced with permission from Reference [114] Copyright 2019, Springer Nature.

To further improve the performance of $\beta''\text{-Al}_2\text{O}_3$ in NMBs, Lei et al. designed a hybridization of inorganic ionic conductors and polymer electrolytes [114]. They used a poly(vinylidene fluoride-co-hexafluoropropylene) (PVDF-HFP)-based polymer to coat $\beta''\text{-Al}_2\text{O}_3$ nanowires (ANs-PVDF-HFP) with uniform cross-linking. Figure 5h shows the SEM images of the ANs-PVDF-HFP membrane. It was found that cross-linked $\beta''\text{-Al}_2\text{O}_3$ nanowires were embedded into the PVDF-HFP matrix. From the cross-sectional SEM image (Figure 5i), the homogeneous and regular pores could be observed in the ANs-PVDF-HFP membrane. It was suggested that the homogeneous and regular pores could store the electrolyte, which was beneficial to shortening the Na-ion migration route and enhancing the ionic conductivity. In addition, the excellent contact and adhesion between the $\beta''\text{-Al}_2\text{O}_3$ nanowires and PVDF-HFP were also observed from the enlarged cross-sectional SEM image in Figure 5j. Due to this structure, the ANs-PVDF-HFP could provide dense and homogeneous Na-ion transportation channels, which facilitated the homogeneous Na metal deposition and decreased the growth of the Na dendrite. Therefore, when the $\text{Na}_3\text{V}_2(\text{PO}_4)_3$ cathode/Na full battery used ANs-PVDF-HFP as the electrolyte, very high capacity retentions of 95.3% and 78.8% after 1000 cycles at 1 C at 25 and $60\text{ }^{\circ}\text{C}$, respectively, were observed.

In addition, another type of all-solid-state electrolyte of the Na superionic conductors (NASICONs, $\text{Na}_3\text{Zr}_2\text{Si}_2\text{PO}_{12}$) ceramic electrolyte was also receiving great attention due to the high ionic conductivity and excellent electrochemical stability [53]. However, the pristine NASICON always exhibited a large interfacial resistance and poor interface wettability for the Na metal anode. Despite this, the scientists also found that they could improve their performance by modifying NASICON solid-state electrolytes. Li et al. developed a method of direct growth of ultrathin graphene-like on the $\text{Na}_3\text{Zr}_2\text{Si}_2\text{PO}_{12}$ (G-NASICON) ceramic electrolyte, which could reduce the interfacial resistance and enable the Na-ion flux with homogeneity across from the G-NASICON ceramic electrolyte to the Na metal anode [115]. Due to this modification, the $\text{Na} \parallel \text{Na}$ symmetric battery in G-NASICON ceramic electrolyte presented a stable cycle performance over 1000 h at 0.5 mA cm^{-2} with the capacity of 1 mAh cm^{-2} . Due to the close interface contact, it was critical to the electrolyte

with a cathode and Na metal anode and a high capacity of 106 mAh g^{-1} could be received in the initial cycle with the $\text{Na}_3\text{V}_2(\text{PO}_4)_3$ cathode.

To realize the all-solid-state Na metal batteries, inorganic–organic hybridization of solid-state electrolytes was one of the routes. Matios et al. reported a hybrid solid-state electrolyte with $\text{Na}_3\text{Zr}_2\text{Si}_2\text{PO}_12$ (NZSP), polypropylene carbonate (PPC), and PEO host (NZSP-PPC-PEO) [52]. They found that Na metal could turn PPC from a long chain polymer into shorter chain segments spontaneously, resulting in the formation of a highly conductive interfacial-wetting layer. Therefore, this phenomenon was utilized to formulate NZSP and PEO host by the content of PPC, as shown in Figure 6a. Due to the highly conductive interfacial-wetting layer, the interfacial conductivity of solid-state electrolytes could be remarkably improved, which resulted in the stable cycling performance (1000 h , 0.1 mA cm^{-2} , 0.1 mAh cm^{-2}) in the $\text{Na} \parallel \text{Na}$ symmetric battery. Ling et al. developed an interpenetrating network of poly(ether-acrylate) (ipN-PEA) in NZSP ceramic/poly(vinylidene fluoride-hexafluoropropylene) (NZSP/PVDF-HFP) with sandwich structure (CESS) as a flexible solid-state electrolyte [116]. They found that this flexible solid-state electrolyte presented an excellent Na-ion transference number of 0.63 and a high ionic conductivity of $10^{-4} \text{ S cm}^{-1}$. In the $\text{Na} \parallel \text{Na}$ symmetric battery, a low polarization voltage of $\pm 50 \text{ mV}$ after 400 h at 0.2 mA cm^{-2} was delivered in the CESS flexible solid-state electrolyte, which presented much better performance than that in liquid electrolytes. They suggested that the improved electrochemical performance of the Na metal anode in the CESS flexible solid-state electrolyte was due to the internal rigidity and external flexibility, resulting in the mitigation of interfacial ion transfer issues and the guarantee of mechanical strength. These behaviors would contribute to the inhibition of Na dendrite growth and dead Na formation. Yu et al. reported a synthetic strategy of NZSP ceramic microtubes with cotton fiber template [117]. After that, they used NZSP ceramic microtubes with poly(ethylene oxide) (PEO)-PVdF-HFP-NaClO₄-1-ethyl-3-methylimidazolium bis(fluorosulfonyl)imide (EmimFSI) (NZSP/PPE) for hybridization to develop an inorganic-organic solid-state electrolyte. After hybridization, this type of solid-state electrolyte presented an electrochemical window of 5.0 V and a transference number of 0.882 with electrical conductivity of $2.79 \times 10^{-4} \text{ S cm}^{-1}$. Due to these characters, the inorganic-organic solid-state electrolyte in the $\text{Na} \parallel \text{Na}$ symmetric battery could be cycling for 200 h at 0.05 mA cm^{-2} .

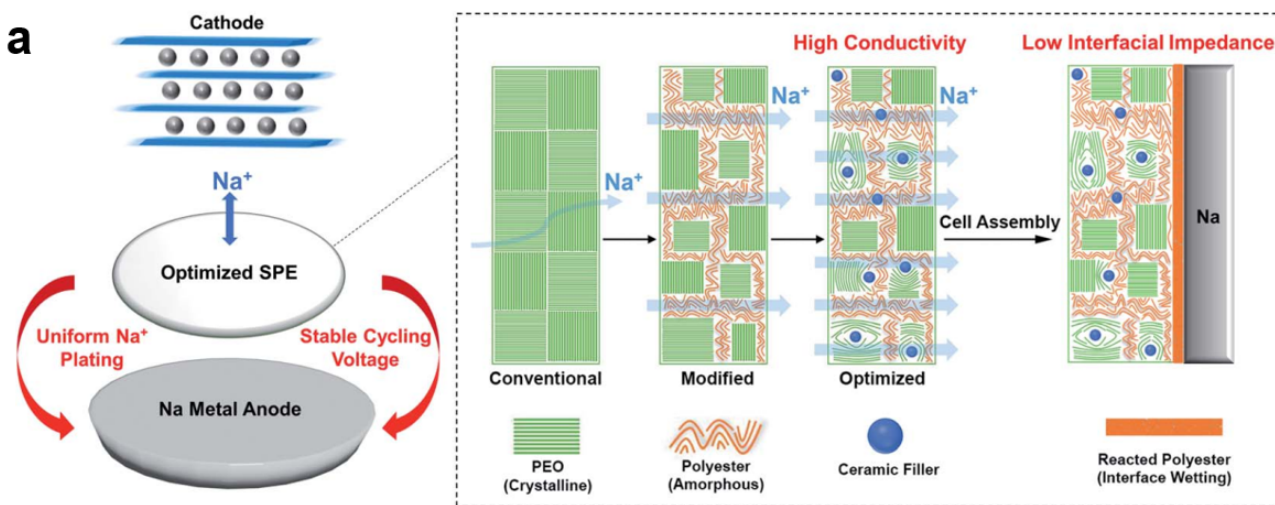


Figure 6. Cont.

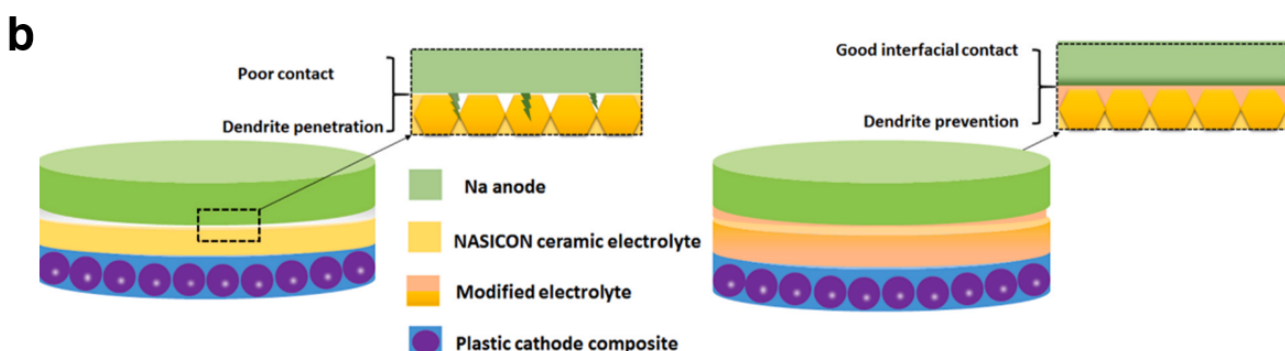


Figure 6. (a) Schematic of the optimizing steps for the proposed composite SPE, reproduced with permission from Reference [52] Copyright 2021, Royal Society of Chemistry. (b) Illustration of the grain boundary engineered ceramic electrolyte depressing the Na dendrites in all-solid-state NMBs, reproduced with permission from Reference [118] Copyright 2021, Elsevier.

In addition, another route was mixing part of the inorganic conductor into NZSP ceramic electrolyte to enhance the contact between the electrolyte and electrode. Figure 6b shows the illustration of the grain boundary engineered ceramic electrolyte to improve the electrochemical performance of the Na metal anode. Zhao et al. utilized $\text{Na}_2\text{B}_4\text{O}_7$ as an additive to modify the NZSP ceramic electrolyte and found that 10 wt% $\text{Na}_2\text{B}_4\text{O}_7$ additives in the NZSP ceramic could enhance the conductivity of 1.72 mS cm^{-1} at RT [118]. With the modification of NZSP ceramic electrolyte, the $\text{Na} \parallel \text{Na}$ symmetric battery presented ultra-stable Na plating–stripping cycling over 2500 h at 0.3 mA cm^{-2} . They found that this modification of the ceramic electrolyte triggered kinetically stable interphase between the electrolyte and Na metal anode, resulting in the reduction of the interfacial resistance for $90 \Omega \text{ cm}^2$ for NZSP to $36 \Omega \text{ cm}^2$ for NZSP-10 wt% $\text{Na}_2\text{B}_4\text{O}_7$. Yang et al. introduced SnO_x/Sn film in the NZSP ceramic to enhance the interface between the Na metal anode and electrolyte [119]. As a result, a remarkable decrease in interfacial resistance from $581 \Omega \text{ cm}^2$ for NZSP to $3 \Omega \text{ cm}^2$ for SnO_x/Sn -NZSP was observed. Due to the decrease in the interfacial resistance, the $\text{Na} \parallel \text{Na}$ symmetric battery in the SnO_x/Sn -NZSP electrolyte maintained cycling over 1500 h with a polarization of $\pm 40 \text{ mV}$ at 0.1 mA cm^{-2} at RT. The symmetric battery still held an excellent cyclability at the large current densities of 0.3 and 0.5 mA cm^{-2} . After being coupled with the cathode, the full batteries also presented a good electrochemical performance at 0.1 and 0.2 C. Wang et al. constructed a stable mixed-ion-electron conductor layer consisting of NaSn alloy and Na_2S on NZSP, which was induced by the introduction of a SnS_2 ultra-thin layer [120]. Based on this construction of the stable interface, the $\text{Na} \parallel \text{Na}$ symmetric battery operated with a low polarization of $\pm 25 \text{ mV}$ at 0.1 mA cm^{-2} at RT during the cycling of 800 h. In addition, the full battery matching $\text{Na}_3\text{V}_2(\text{PO}_4)_3$ cathode in the SnO_x/Sn -NZSP electrolyte also delivered a superior capacity retention ratio. They suggested that the SnS_2 could immerse the grain boundaries and voids of NZSP, which avoided the immediate contact between the Na metal anode and NZSP. In addition, the NaSn alloy was also formed during the Na metal deposition, which endowed the good wettability between the Na anode and NZSP and reduced the interfacial impedance. Furthermore, the mixed-ion-electron conductor layer on NZSP also realized the homogeneous and rapid Na-ion flux transfer from the interface, resulting in uniform Na metal deposition.

Interface modification was also another strategy to improve interface resistance between the electrolyte and electrode [53,121]. Therefore, Wang et al. adopted a surface potential regulation strategy to mitigate the interfacial potential divergence and modify the Na/NZSP interface through the active control of the ceramic electrolyte surface microstructure [121]. The surface regulation of the Na/NZSP interface presented stability for over 4 months with the interfacial resistance of $129 \Omega \text{ cm}^2$ at 25°C . To understand the modification of the $\text{Na}_3\text{Zr}_2\text{Si}_2\text{PO}_12$ interface, they conducted the in-depth ToF-SIMS

mapping of the interface after Na metal plating/stripping, as shown in Figure 7. Na metal islands (Figure 7a) and Na dendrite (Figure 7b) with tens of millimeters could be observed in the NZSP electrolyte without interface modification. With the interface modification, the Na metal anode presented uniform distribution on the surface without Na dendrite (Figure 7c,d). These results were also demonstrated in the SEM image.

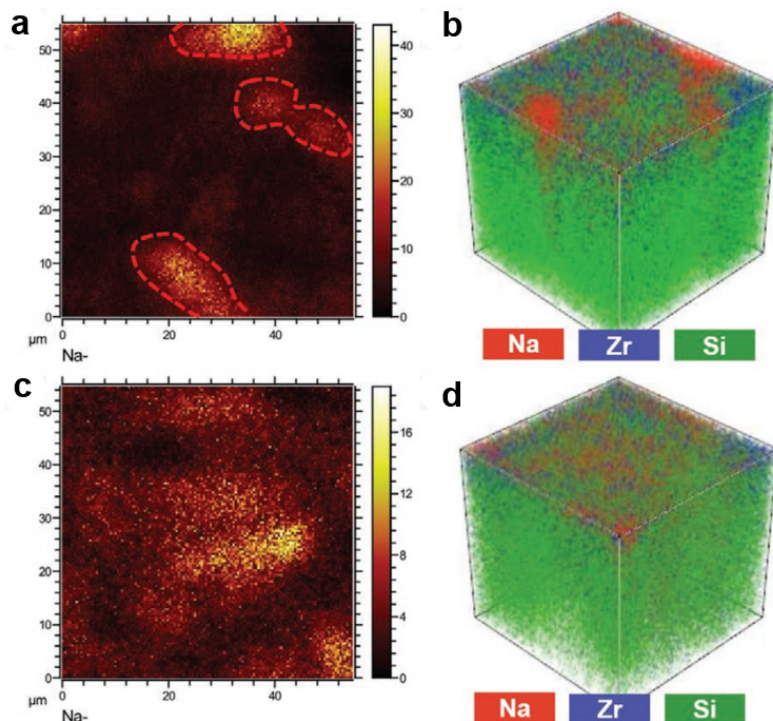


Figure 7. (a) Mapping of Na species and (b) overlay depth profile of Na, Zr, and Si on TS1300-15/1200 after cycling; (c) mapping of Na species and (d) overlay depth profile of Na, Zr, and Si on NS1250 after cycling, reproduced with permission from Reference [121] Copyright 2021, Elsevier.

Except for $\text{Na}-\beta''-\text{Al}_2\text{O}_3$ and NZSP all-solid-state electrolytes, the other new types of all-solid-state electrolytes for NMBs were also developed. Ruiz-Martinez et al. developed NaY_xNH_3 ($\text{Y} = \text{I}^-$, BF_4^- or BH_4^-) solid-state electrolyte with a high Na-ion concentration ($> 7 \text{ M}$) and high specific conductivity (0.1 S cm^{-1}) for NMBs [122]. They selected three different solid-state electrolytes, $\text{NaI}_{3.3}\text{NH}_3$, $\text{NaBH}_4 \bullet 1.5\text{NH}_3$, and $\text{NaBF}_4 \bullet 2.5\text{NH}_3$ for comparison. It was found that all three ammonia-based electrolytes in NMBs exhibited stability for several weeks and retained a CE of close to 100% and high cyclability even at a large current of 10 mA cm^{-2} . To compare the electrochemical performance of these solid-state electrolytes in NMBs, the $\text{Cu} \parallel \text{Na}$ asymmetric battery in $\text{NaI}_{3.3}\text{NH}_3$, $\text{NaBH}_4 \bullet 1.5\text{NH}_3$, and $\text{NaBF}_4 \bullet 2.5\text{NH}_3$ electrolytes were also measured. A low voltage hysteresis of $\pm 4.5 \text{ mV}$ and high Na reversibility for the $\text{NaBF}_4 \bullet 2.5\text{NH}_3$ electrolyte could be achieved in NMBs, indicating that solid-state ammonia-based electrolytes were feasible.

There are also some practical applications for all-solid-state electrolytes. All-solid-state $\text{Na}-\text{O}_2$ batteries had great development potential due to their high energy density and high safety [123,124]. Liu et al. reported an all-solid-state $\text{Na}-\text{O}_2$ battery based on a well-designed NASICON-type electrolyte $\text{Na}_{3.2}\text{Hf}_2\text{Si}_{2.2}\text{P}_{0.8}\text{O}_{11.85}\text{F}_{0.3}$, which has high ionic conductivity ($2.39 \times 10^{-3} \text{ S cm}^{-1}$) and excellent chemical stability [125]. In addition, a proposed $\text{Na}-\text{O}_2$ battery was successfully constructed using an NASICON structured solid electrolyte and a liquid anode, which demonstrated low voltage gap, reversibility, and high safety [126]. Sun et al. successfully developed a hybrid solid-state $\text{Na}-\text{O}_2$ battery based on the NASICON solid-state electrolyte (SSE) and Na anode protected by carbon paper (CP). Owing to the combined advantages of SSE and CP modification, the developed $\text{Na}-\text{O}_2$

battery delivered high discharge capacities with excellent coulombic efficiency as well as stable cycling performance [123].

In addition, soft breakdown phenomena in all-solid-state symmetric batteries were pretty common because of the high electronic conductivity of solid-state electrolytes, poor interfacial solid–solid ionic contact, and uneven localized electric field. However, soft breakdown hidden in all-solid-state NMBs had been overlooked in most previous research. This abnormal phenomenon had significantly retarded the progress of improving Na metal anodes for practical engineering of all-solid-state NMBs. Sun et al. proposed a simple but effective strategy—cyclic voltammetry (CV)—to diagnose soft breakdown in all-solid-state symmetric batteries [127]. The charge carrier of an all-solid-state symmetric battery should be only ions. If an all-solid-state symmetric cell had both ion and electron transport, it was a soft breakdown. For all-solid-state symmetric batteries with soft breakdown, CV would show a mixed state of both electrochemical process and electronic conduction. Therefore, CV was a simple but effective method to diagnose the soft breakdown phenomenon in all-solid-state symmetric NMBs. It was necessary for all-solid-state NMBs to avoid arbitrary testing parameters and ignorance of soft breakdown in the future.

Based on the above discussion, we summarized the electrochemical properties of modified all-solid-state electrolytes for NMBs and listed some important parameters including ionic conductivity, and cycling stability of recent works, as shown in Table 3.

Table 3. Electrochemical properties of different all-solid-state electrolytes in NMBs.

All-Solid-State Electrolytes	Ionic Conductivity (mS cm ⁻¹)@Temperature (°C)	Symmetrical Cell (Cycle Performance (h)@Current Density (mA cm ⁻²))	Full Cell (Cathode@Capacity (mAh g ⁻¹)@Current Density (C))	References
Na-β''-Al ₂ O ₃	2.1@RT	/	/	[110]
BASE-CNT	0.36@58	1000@0.1	Na ₃ V ₂ (PO ₄) ₃ @100.6@0.1 O ₃ ⁻	[111]
YSZ/BASE	0.46@RT	330@0.5	NaNi _{0.45} Cu _{0.05} Mn _{0.4} Ti _{0.1} O ₂ @110@1 PTO-PEO@180@0.5	[112]
Sn-BASE	1.1@60	1000@0.5	Na ₃ V ₂ (PO ₄) ₃ @108@1	[113]
G-NASICON	0.6@RT	1000@0.5	Na ₃ V ₂ (PO ₄) ₃ @102@1	[115]
NZSP-PPC-PEO	0.12@RT	1000@0.1	Na ₃ V ₂ (PO ₄) ₃ @95@0.2	[52]
NZSP/PVDF-HFP	0.132@60	400@0.2	Na ₃ V ₂ (PO ₄) ₃ @95@0.2	[116]
NZSP/PPE	0.693@25	200@0.05	Na _{0.67} Ni _{0.33} Mn _{0.67} O ₂ @112@0.1 Y-Na ₂ O ₃ Zr/C@90.5@0.05	[117]
PEO-NaClO ₄ -SiO ₂ -Emim FSI	1.3@RT	/	Y-Na ₂ O ₃ Zr/C@90.5@0.05	[128]
NZSP-Na ₂ B ₄ O ₇	1.72@RT	2500@0.3	Na ₃ V _{1.5} Cr _{0.5} (PO ₄) ₃ @107@30 mA g ⁻¹	[118]
TiO ₂ -NZSP	0.53@25	860@0.1	Na ₃ V ₂ (PO ₄) ₃ @103.1@0.2	[129]
Ca-NZSP	1.67@25	600@0.3	Na ₃ Ti ₂ (PO ₄) ₃ @96.4@0.2	[130]
SnO _x /Sn/NZSP	0.59@RT	1500@0.1	Na ₃ V ₂ (PO ₄) ₃ @101.2@0.5	[119]
SnS ₂ /NZSP	0.42@RT	800@0.1	Na ₃ V ₂ (PO ₄) ₃ @85.5@0.5	[120]
ANs-GPE	0.713@25	300@1	Na ₃ V ₂ (PO ₄) ₃ @114.6@0.2	[114]
NZSP	0.85@RT	1000@0.2	Na ₃ V _{1.5} Cr _{0.5} (PO ₄) ₃ @111@1	[121]
AlF ₃ /NZSP	0.2415@RT	150@0.15	Na ₃ V ₂ (PO ₄) ₃ @110@0.2	[131]
H-NASICON	0.07@65	550@0.25	NaTi ₂ (PO ₄) ₃ @110@0.2	[96]

Considering the practical application of NMBs in the future, NMBs design should not be limited to coin batteries. Currently, three major cell formats are commercially used: cylindrical, prismatic, and pouch. Among them, the pouch cells based on layered constructions allow maximum use of space and active materials and therefore are popular for large cell formats [132]. However, the excessive capacities and thicknesses of the available Na metal foils remain a critical yet unresolved challenge in practical pouch cells. Practical Na metal pouch cells require a ultra-thin Na metal foil paired with the conventional cathode to satisfy a lower negative to positive areal capacity (N/P) ratio [133]. The existing technology cannot satisfy the requirements of ultra-thin sodium metal anodes. Thus, the side reactions in the pouch cells with a high excess of Na may be intensified. New manufacturing capabilities will be needed to control the thickness of the Na metal anodes in the future. In addition, a higher CE close to 100% could be enabled by an electrolyte that produces a more stable SEI and fewer side reactions, or by an anode that allows a

more stable interface such as a surface protection layer to reduce the interactions with the electrolytes [134].

5. Conclusions and Perspectives

Electrolyte optimization was a simple and easy solution to address the dendrite growth and unstable SEI layer of Na anodes limiting the development of NMBs, and a method that could effectively protect Na-metal anodes and avoid unstable SEI layer formation and dendrite growth. Common liquid electrolyte optimization methods included the replacement of solvent, replacement of Na salt and electrolyte additives, etc. For liquid electrolytes, the choice of Na salts and solvents was crucial, as they largely determined the composition of the SEI layer and greatly changed the Na ion migration path. At the same time, the use of additives in the electrolytes could also tune the SEI layer composition, which was critical for the formation of a stable and continuous SEI layer. In addition, increasing electrolyte concentration could also build a stable SEI layer and inhibit dendrite growth. However, the high cost, high viscosity, and low electrical conductivity hindered its practical application. To solve this problem, the concept of local high-concentration electrolyte was proposed, that was, adding diluent to the high-concentration electrolyte to reduce the Na salt concentration of the electrolyte, which could improve the ionic conductivity while building a stable SEI layer.

Except for liquid electrolytes, we also discussed the relevant strategies related to solid-state electrolytes for enhancement of electrochemical performance. We found that the polymer electrolytes and all-solid-state electrolytes could settle some critical issues such as dendritic growth, resulting in a decrease in the assembly process and an increase in the safety of NMBs. However, high interface impedance and low Na-ion mobility still restrain the application in NMBs. All the polymer electrolytes and all-solid-state electrolytes mainly were devoted to addressing the interface impedance and low Na-ion mobility. One was the exploration of host material with high Na-ion mobility. However, most host materials could not achieve good interface contact. Interface modification, hybridization of the organic and inorganic host material, Na-ion channel adjustment, etc., were the alternative measures to improve the electrochemical performance of Na metal anodes in polymer or all-solid-state electrolytes. Despite these efforts, the relatively large polarization voltages of NMBs in solid-state electrolytes were still existed. Continuous research was needed to promote the further development and application of NMBs.

For the liquid electrolytes, great progress has been made in the optimization at present, but the spontaneous reaction between the Na metal anode and liquid electrolyte cannot be completely suppressed, which will inevitably lead to the growth of Na dendrites. In the future, more solutions need to be proposed to stabilize the Na metal anodes, such as finding a solvent with a higher LUMO energy level that could reduce the reaction between the electrolyte and the Na metal, resulting in a stable SEI layer; finding a consideration of the substitution with flammable liquid electrolytes to improve the safety of NMBs. In addition, considering the limitation of a single strategy by electrolyte engineering, comprehensive strategies combined with the introduction of host materials for Na metal anodes, an artificial SEI layer onto Na metal anodes, should be feasible to improve the electrochemical performance of Na metal anodes. Certainly, our ultimate goal is the development of solid-state NMBs, and the improvement of the performance of polymer or all-solid-state electrolytes becomes the research emphasis. Although a lot of excellent works related to polymer or all-solid-state electrolytes have been undertaken, the conductivity issue at RT has not been solved effectively. In addition, interfacial compatibility issues between the electrolyte and electrode have not been resolved effectivity. To further address these issues, we suggest that a hybridization strategy to construct a 3D interconnected ceramic framework can offer a rapid Na-ion transport path, which can enhance the electrochemical stability of NMBs. In addition, to address the interfacial compatibility between electrolyte and electrode, the construction of the novel solid-state electrolytes, functional gradient solid-state electrolytes, multilayer ceramic electrolytes, etc., are still necessary to explore for

NMBs. Moreover, simply optimizing the solid-state electrolytes in NMBs from a technical level cannot effectively improve the performance of the Na metal anodes. Therefore, further revealing the potential electrochemical mechanisms, including the Na-ion transport behaviors, transfer paths, internal interactions, etc., is also crucial. This understanding will be favorable to guide the design of a new type of solid-state electrolytes with high ionic conductivity and optimization of the configuration and composition of the solid-state electrolytes.

Funding: This research is funded by [Shenzhen Science and Technology Program] grant number [JCYJ20200109113606007] and [Science and Technology Program of Guangzhou] grant number [202102020737].

Data Availability Statement: Not applicable.

Acknowledgments: We also thank the financial support from the Shenzhen Science and Technology Program (JCYJ20200109113606007) and the Science and Technology Program of Guangzhou, China (202102020737).

Conflicts of Interest: The authors declare no conflict of interest.

References

- Wen, J.; Zhao, D.; Zhang, C. An overview of electricity powered vehicles: Lithium-ion battery energy storage density and energy conversion efficiency. *Renew. Energy* **2020**, *162*, 1629–1648. [[CrossRef](#)]
- Wang, Z.; Zhuo, W.; Li, J.; Ma, L.; Tan, S.; Zhang, G.; Yin, H.; Qin, W.; Wang, H.; Pan, L. Regulation of ferric iron vacancy for Prussian blue analogue cathode to realize high-performance potassium ion storage. *Nano Energy* **2022**, *98*, 107243. [[CrossRef](#)]
- Dai, L.; Huang, K.; Xia, Y.; Xu, Z. Two-dimensional material separation membranes for renewable energy purification, storage, and conversion. *Green Energy Environ.* **2021**, *6*, 193–211. [[CrossRef](#)]
- Li, J.L.; Zhuang, N.; Xie, J.P.; Li, X.D.; Zhuo, W.C.; Wang, H.; Na, J.B.; Li, X.B.; Yamauchi, Y.; Mai, W.J. K-Ion Storage Enhancement in Sb_2O_3 /Reduced Graphene Oxide Using Ether-Based Electrolyte. *Adv. Energy Mater.* **2020**, *10*, 1903455. [[CrossRef](#)]
- Hirsh, H.S.; Li, Y.; Tan, D.H.; Zhang, M.; Zhao, E.; Meng, Y.S. Sodium-ion batteries paving the way for grid energy storage. *Adv. Energy Mater.* **2020**, *10*, 2001274. [[CrossRef](#)]
- Choi, D.; Shamim, N.; Crawford, A.; Huang, Q.; Vartanian, C.K.; Viswanathan, V.V.; Paiss, M.D.; Alam, M.J.E.; Reed, D.M.; Sprenkle, V.L. Li-ion battery technology for grid application. *J. Power Sources* **2021**, *511*, 230419. [[CrossRef](#)]
- Vivo-Vilches, J.F.; Karakashov, B.; Celzard, A.; Fierro, V.; El Hage, R.; Brosse, N.; Dufour, A.; Etienne, M. Carbon Monoliths with Hierarchical Porous Structure for All-Vanadium Redox Flow Batteries. *Batteries* **2021**, *7*, 55. [[CrossRef](#)]
- Zhou, J.; Zhuang, H.L.; Wang, H. Layered tetragonal zinc chalcogenides for energy-related applications: From photocatalysts for water splitting to cathode materials for Li-ion batteries. *Nanoscale* **2017**, *9*, 17303–17311. [[CrossRef](#)]
- Gao, L.; Chen, S.; Zhang, G.; Dai, Z.; Yan, D.; Yang, H.Y.; Yu, C.; Bai, Y. Improved thermal and structural stabilities of $\text{LiNi}_{0.6}\text{Co}_{0.2}\text{Mn}_{0.2}\text{O}_2$ cathode by $\text{La}_2\text{Zr}_2\text{O}_7$ multifunctional modification. *Appl. Phys. Lett.* **2021**, *119*, 093902. [[CrossRef](#)]
- Nisar, U.; Muralidharan, N.; Essehli, R.; Amin, R.; Belharouak, I. Valuation of surface coatings in high-energy density lithium-ion battery cathode materials. *Energy Storage Mater.* **2021**, *38*, 309–328. [[CrossRef](#)]
- Xie, J.P.; Li, X.D.; Lai, H.J.; Zhao, Z.J.; Li, J.L.; Zhang, W.G.; Xie, W.G.; Liu, Y.M.; Mai, W.J. A Robust Solid Electrolyte Interphase Layer Augments the Ion Storage Capacity of Bimetallic-Sulfide-Containing Potassium-Ion Batteries. *Angew. Chem. Int. Ed.* **2019**, *58*, 14740–14747. [[CrossRef](#)] [[PubMed](#)]
- Xie, J.; Li, J.; Li, X.; Lei, H.; Zhuo, W.; Li, X.; Hong, G.; Hui, K.N.; Pan, L.; Mai, W. Ultrahigh “relative energy density” and mass loading of carbon cloth anodes for K-ion batteries. *CCS Chem.* **2021**, *3*, 791–799. [[CrossRef](#)]
- Ma, K.; Liu, Y.; Jiang, H.; Hu, Y.; Si, R.; Liu, H.; Li, C. Multivalence-ion intercalation enables ultrahigh 1T phase MoS_2 nanoflowers to enhanced sodium-storage performance. *CCS Chem.* **2021**, *3*, 1472–1482. [[CrossRef](#)]
- Mohsin, I.U.; Ziebert, C.; Rohde, M.; Seifert, H.J. Thermophysical characterization of a layered P2 type structure $\text{Na}_{0.53}\text{MnO}_2$ cathode material for sodium ion batteries. *Batteries* **2021**, *7*, 16. [[CrossRef](#)]
- Li, X.D.; Liu, Z.B.; Li, J.L.; Lei, H.; Zhuo, W.C.; Qin, W.; Cai, X.; Hui, K.N.; Pan, L.K.; Mai, W.J. Insights on the mechanism of Na-ion storage in expanded graphite anode. *J. Energy Chem.* **2021**, *53*, 56–62. [[CrossRef](#)]
- Dong, S.; Lv, N.; Wu, Y.; Zhang, Y.; Zhu, G.; Dong, X. Titanates for sodium-ion storage. *Nano Today* **2022**, *42*, 101349. [[CrossRef](#)]
- Yang, C.; Xin, S.; Mai, L.; You, Y. Materials design for high-safety sodium-ion battery. *Adv. Energy Mater.* **2021**, *11*, 2000974. [[CrossRef](#)]
- Lyu, T.; Lan, X.; Liang, L.; Lin, X.; Hao, C.; Pan, Z.; Tian, Z.Q.; Shen, P.K. Natural mushroom spores derived hard carbon plates for robust and low-potential sodium ion storage. *Electrochim. Acta* **2021**, *365*, 137356. [[CrossRef](#)]
- Liu, Q.; Xu, R.; Mu, D.; Tan, G.; Gao, H.; Li, N.; Chen, R.; Wu, F. Progress in electrolyte and interface of hard carbon and graphite anode for sodium-ion battery. *Carbon Energy* **2022**, *4*, 458–479. [[CrossRef](#)]

20. Maça, R.R.; Etacheri, V. Effect of vinylene carbonate electrolyte additive on the surface chemistry and pseudocapacitive sodium-ion storage of TiO₂ nanosheet anodes. *Batteries* **2020**, *7*, 1. [[CrossRef](#)]
21. Chu, C.; Li, R.; Cai, F.; Bai, Z.; Wang, Y.; Xu, X.; Wang, N.; Yang, J.; Dou, S. Recent advanced skeletons in sodium metal anodes. *Energy Environ. Sci.* **2021**, *14*, 4318–4340. [[CrossRef](#)]
22. Yuan, X.R.; Chen, S.M.; Li, J.L.; Xie, J.P.; Yan, G.H.; Liu, B.T.; Li, X.B.; Li, R.; Pan, L.K.; Mai, W.J. Understanding the improved performance of sulfur-doped interconnected carbon microspheres for Na-ion storage. *Carbon Energy* **2021**, *3*, 615–626. [[CrossRef](#)]
23. Zhang, Y.J.; Li, J.L.; Ma, L.; Li, H.B.; Xu, X.T.; Liu, X.J.; Lu, T.; Pan, L.K. Insights into the storage mechanism of 3D nanoflower-like V₃S₄ anode in sodium-ion batteries. *Chem. Eng. J.* **2022**, *427*, 130936. [[CrossRef](#)]
24. Sun, Y.; Yang, Y.; Shi, X.-L.; Suo, G.; Xue, F.; Liu, J.; Lu, S.; Chen, Z.-G. N-doped silk wadding-derived carbon/SnO_x@ reduced graphene oxide film as an ultra-stable anode for sodium-ion half/full battery. *Chem. Eng. J.* **2022**, *433*, 133675. [[CrossRef](#)]
25. Park, J.; Sharma, J.; Jafta, C.J.; He, L.; Meyer III, H.M.; Li, J.; Keum, J.K.; Nguyen, N.A.; Polizos, G. Reduced Graphene Oxide Aerogels with Functionalization-Mediated Disordered Stacking for Sodium-Ion Batteries. *Batteries* **2022**, *8*, 12. [[CrossRef](#)]
26. Jiang, B.; Wei, Y.; Wu, J.; Cheng, H.; Yuan, L.; Li, Z.; Xu, H.; Huang, Y. Recent progress of asymmetric solid-state electrolytes for lithium/sodium-metal batteries. *EnergyChem* **2021**, *3*, 100058. [[CrossRef](#)]
27. Fang, H.Y.; Gao, S.N.; Zhu, Z.; Ren, M.; Wu, Q.; Li, H.X.; Li, F.J. Recent Progress and Perspectives of Sodium Metal Anodes for Rechargeable Batteries. *Chem. Res. Chin. Univ.* **2021**, *37*, 189–199. [[CrossRef](#)]
28. Li, Z.P.; Zhu, K.J.; Liu, P.; Jiao, L.F. 3D Confinement Strategy for Dendrite-Free Sodium Metal Batteries. *Adv. Energy Mater.* **2022**, *12*, 210359. [[CrossRef](#)]
29. Bao, C.Y.; Wang, B.; Liu, P.; Wu, H.; Zhou, Y.; Wang, D.L.; Liu, H.K.; Dou, S.X. Solid Electrolyte Interphases on Sodium Metal Anodes. *Adv. Funct. Mater.* **2020**, *30*, 2004891. [[CrossRef](#)]
30. Chen, Q.W.; He, H.; Hou, Z.; Zhuang, W.M.; Zhang, T.X.; Sun, Z.Z.; Huang, L.M. Building an artificial solid electrolyte interphase with high-uniformity and fast ion diffusion for ultralong-life sodium metal anodes. *J. Mater. Chem. A* **2020**, *8*, 16232–16237. [[CrossRef](#)]
31. Zhao, Y.; Goncharova, L.V.; Lushington, A.; Sun, Q.; Yadegari, H.; Wang, B.Q.; Xiao, W.; Li, R.Y.; Sun, X.L. Superior Stable and Long Life Sodium Metal Anodes Achieved by Atomic Layer Deposition. *Adv. Mater.* **2017**, *29*, 1606663. [[CrossRef](#)] [[PubMed](#)]
32. Lee, J.; Kim, J.; Kim, S.; Jo, C.; Lee, J. A review on recent approaches for designing the SEI layer on sodium metal anodes. *Mater. Adv.* **2020**, *1*, 3143–3166. [[CrossRef](#)]
33. Wang, H.; Liang, J.L.; Wu, Y.; Kang, T.X.; Shen, D.; Tong, Z.Q.; Yang, R.; Jiang, Y.; Wu, D.; Li, X.J.; et al. Porous BN Nanofibers Enable Long-Cycling Life Sodium Metal Batteries. *Small* **2020**, *16*, 2002671. [[CrossRef](#)] [[PubMed](#)]
34. Zhang, Q.; Lu, Y.Y.; Miao, L.C.; Zhao, Q.; Xia, K.X.; Liang, J.; Chou, S.L.; Chen, J. An Alternative to Lithium Metal Anodes: Non-dendritic and Highly Reversible Sodium Metal Anodes for Li-Na Hybrid Batteries. *Angew. Chem. Int. Ed.* **2018**, *57*, 14796–14800. [[CrossRef](#)]
35. Wang, H.; Wu, Y.; Liu, S.; Jiang, Y.; Shen, D.; Kang, T.; Tong, Z.; Wu, D.; Li, X.; Lee, C.S. 3D Ag@C cloth for stable anode free sodium metal batteries. *Small Methods* **2021**, *5*, 2001050. [[CrossRef](#)] [[PubMed](#)]
36. Li, L.; Zhu, M.; Wang, G.; Yu, F.; Wen, L.; Liu, H.-K.; Dou, S.-X.; Wu, C. An in-situ generated Bi-based sodiophilic substrate with high structural stability for high-performance sodium metal batteries. *J. Energy Chem.* **2022**, *71*, 595–603. [[CrossRef](#)]
37. Liang, J.; Wu, W.; Xu, L.; Wu, X. Highly stable Na metal anode enabled by a multifunctional hard carbon skeleton. *Carbon* **2021**, *176*, 219–227. [[CrossRef](#)]
38. Mo, L.; Chen, A.-L.; Ouyang, Y.; Zong, W.; Miao, Y.-E.; Liu, T. Asymmetric Sodiophilic Host Based on a Ag-Modified Carbon Fiber Framework for Dendrite-Free Sodium Metal Anodes. *ACS Appl. Mater. Interfaces* **2021**, *13*, 48634–48642. [[CrossRef](#)]
39. Yang, W.; Yang, W.; Dong, L.; Shao, G.; Wang, G.; Peng, X. Hierarchical ZnO nanorod arrays grown on copper foam as an advanced three-dimensional skeleton for dendrite-free sodium metal anodes. *Nano Energy* **2021**, *80*, 105563. [[CrossRef](#)]
40. Ye, S.; Wang, L.; Liu, F.; Shi, P.; Yu, Y. Integration of homogeneous and heterogeneous nucleation growth via 3D alloy framework for stable Na/K metal anode. *eScience* **2021**, *1*, 75–82. [[CrossRef](#)]
41. Liu, T.; Yang, X.; Nai, J.; Wang, Y.; Liu, Y.; Liu, C.; Tao, X. Recent development of Na metal anodes: Interphase engineering chemistries determine the electrochemical performance. *Chem. Eng. J.* **2021**, *409*, 127943. [[CrossRef](#)]
42. Ma, B.; Bai, P. Fast Charging Limits of Ideally Stable Metal Anodes in Liquid Electrolytes. *Adv. Energy Mater.* **2022**, *12*, 2102967. [[CrossRef](#)]
43. Zhao, W.; Guo, M.; Zuo, Z.; Zhao, X.; Dou, H.; Zhang, Y.; Li, S.; Wu, Z.; Shi, Y.; Ma, Z. Engineering sodium metal anode with sodiophilic bismuthide penetration for dendrite-free and high-rate sodium-ion battery. *Engineering* **2022**, *11*, 87–94. [[CrossRef](#)]
44. Zheng, X.; Gu, Z.; Fu, J.; Wang, H.; Ye, X.; Huang, L.; Liu, X.; Wu, X.; Luo, W.; Huang, Y. Knocking down the kinetic barriers towards fast-charging and low-temperature sodium metal batteries. *Energy Environ. Sci.* **2021**, *14*, 4936–4947. [[CrossRef](#)]
45. Wang, S.; Liu, Y.; Lu, K.; Cai, W.; Jie, Y.; Huang, F.; Li, X.; Cao, R.; Jiao, S. Engineering rGO/MXene hybrid film as an anode host for stable sodium-metal batteries. *Energy Fuels* **2021**, *35*, 4587–4595. [[CrossRef](#)]
46. Yang, H.; Zhang, L.; Wang, H.; Huang, S.; Xu, T.; Kong, D.; Zhang, Z.; Zang, J.; Li, X.; Wang, Y. Regulating Na deposition by constructing a Au sodiophilic interphase on CNT modified carbon cloth for flexible sodium metal anode. *J. Colloid Interface Sci.* **2022**, *611*, 317–326. [[CrossRef](#)]
47. Wang, R.; Han, H.-H.; Liu, F.-Q.; Jia, S.-X.; Xiang, T.-Q.; Huo, H.; Zhou, J.-J.; Li, L. Sulfonated poly (vinyl alcohol) as an artificial solid electrolyte interfacial layer for Li metal anode. *Electrochim. Acta* **2022**, *406*, 139840. [[CrossRef](#)]

48. Cheng, Y.; Yang, X.; Li, M.; Li, X.; Lu, X.; Wu, D.; Han, B.; Zhang, Q.; Zhu, Y.; Gu, M. Enabling Ultrastable Alkali Metal Anodes by Artificial Solid Electrolyte Interphase Fluorination. *Nano Lett.* **2022**, *22*, 4347–4353. [[CrossRef](#)]
49. Hu, X.F.; Matios, E.; Zhang, Y.W.; Wang, C.L.; Luo, J.M.; Li, W.Y. Deeply Cycled Sodium Metal Anodes at Low Temperature and in Lean Electrolyte Conditions. *Angew. Chem. Int. Ed.* **2021**, *60*, 5978–5983. [[CrossRef](#)]
50. Wang, Y.; Jiang, R.; Liu, Y.; Zheng, H.; Fang, W.; Liang, X.; Sun, Y.; Zhou, R.; Xiang, H. Enhanced Sodium Metal/Electrolyte Interface by a Localized High-Concentration Electrolyte for Sodium Metal Batteries: First-Principles Calculations and Experimental Studies. *ACS Appl. Energy Mater.* **2021**, *4*, 7376–7384. [[CrossRef](#)]
51. Fang, W.; Jiang, R.; Zheng, H.; Zheng, Y.; Sun, Y.; Liang, X.; Xiang, H.F.; Feng, Y.Z.; Yu, Y. Stable sodium metal anode enhanced by advanced electrolytes with SbF₃ additive. *Rare Met.* **2021**, *40*, 433–439. [[CrossRef](#)]
52. Matios, E.; Wang, H.; Luo, J.; Zhang, Y.; Wang, C.; Lu, X.; Hu, X.; Xu, Y.; Li, W. Reactivity-guided formulation of composite solid polymer electrolytes for superior sodium metal batteries. *J. Mater. Chem. A* **2021**, *9*, 18632–18643. [[CrossRef](#)]
53. Oh, J.A.S.; Wang, Y.M.; Zeng, Q.B.; Sun, J.G.; Sun, Q.M.; Goh, M.; Chua, B.; Zeng, K.Y.; Lu, L. Intrinsic low sodium/NASICON interfacial resistance paving the way for room temperature sodium-metal battery. *J. Colloid Interf. Sci.* **2021**, *601*, 418–426. [[CrossRef](#)] [[PubMed](#)]
54. Xu, P.; Li, X.; Yan, M.-Y.; Ni, H.-B.; Huang, H.-H.; Lin, X.-D.; Liu, X.-Y.; Fan, J.-M.; Zheng, M.-S.; Yuan, R.-M. A highly reversible sodium metal anode by mitigating electrodeposition overpotential. *J. Mater. Chem. A* **2021**, *9*, 22892–22900. [[CrossRef](#)]
55. Zheng, X.; Huang, L.; Ye, X.; Zhang, J.; Min, F.; Luo, W.; Huang, Y. Critical effects of electrolyte recipes for Li and Na metal batteries. *Chem-US* **2021**, *7*, 2312–2346. [[CrossRef](#)]
56. Fan, L.; Li, X. Recent advances in effective protection of sodium metal anode. *Nano Energy* **2018**, *53*, 630–642. [[CrossRef](#)]
57. Matios, E.; Wang, H.; Wang, C.; Li, W. Enabling safe sodium metal batteries by solid electrolyte interphase engineering: A review. *Ind. Eng. Chem. Res.* **2019**, *58*, 9758–9780. [[CrossRef](#)]
58. Oh, J.A.S.; He, L.; Chua, B.; Zeng, K.; Lu, L. Inorganic sodium solid-state electrolyte and interface with sodium metal for room-temperature metal solid-state batteries. *Energy Storage Mater.* **2021**, *34*, 28–44. [[CrossRef](#)]
59. Lee, B.; Paek, E.; Mitlin, D.; Lee, S.W. Sodium Metal Anodes: Emerging Solutions to Dendrite Growth. *Chem. Rev.* **2019**, *119*, 5416–5460. [[CrossRef](#)]
60. Liu, W.; Liu, P.; Mitlin, D. Review of Emerging Concepts in SEI Analysis and Artificial SEI Membranes for Lithium, Sodium, and Potassium Metal Battery Anodes. *Adv. Energy Mater.* **2020**, *10*, 2002297. [[CrossRef](#)]
61. Sun, B.; Xiong, P.; Maitra, U.; Langsdorf, D.; Yan, K.; Wang, C.; Janek, J.; Schroder, D.; Wang, G. Design Strategies to Enable the Efficient Use of Sodium Metal Anodes in High-Energy Batteries. *Adv. Mater.* **2020**, *32*, e1903891. [[CrossRef](#)] [[PubMed](#)]
62. Seh, Z.W.; Sun, J.; Sun, Y.; Cui, Y. A Highly Reversible Room-Temperature Sodium Metal Anode. *ACS Cent. Sci.* **2015**, *1*, 449–455. [[CrossRef](#)] [[PubMed](#)]
63. Zhu, M.; Zhang, Y.; Yu, F.; Huang, Z.; Zhang, Y.; Li, L.; Wang, G.; Wen, L.; Liu, H.K.; Dou, S.X.; et al. Stable Sodium Metal Anode Enabled by an Interface Protection Layer Rich in Organic Sulfide Salt. *Nano Lett.* **2021**, *21*, 619–627. [[CrossRef](#)] [[PubMed](#)]
64. Wang, H.; Yu, Z.; Kong, X.; Kim, S.C.; Boyle, D.T.; Qin, J.; Bao, Z.; Cui, Y. Liquid electrolyte: The nexus of practical lithium metal batteries. *Joule* **2022**, *6*, 588–616. [[CrossRef](#)]
65. Yoon, H.; Zhu, H.J.; Hervault, A.; Armand, M.; MacFarlane, D.R.; Forsyth, M. Physicochemical properties of N-propyl-N-methylpyrrolidinium bis(fluorosulfonyl)imide for sodium metal battery applications. *Phys. Chem. Chem. Phys.* **2014**, *16*, 12350–12355. [[CrossRef](#)]
66. Shi, Q.W.; Zhong, Y.R.; Wu, M.; Wang, H.Z.; Wang, H.L. High-Performance Sodium Metal Anodes Enabled by a Bifunctional Potassium Salt. *Angew. Chem. Int. Ed.* **2018**, *57*, 9069–9072. [[CrossRef](#)]
67. Cao, R.G.; Mishra, K.; Li, X.L.; Qian, J.F.; Engelhard, M.H.; Bowden, M.E.; Han, K.S.; Mueller, K.T.; Henderson, W.A.; Zhang, J.G. Enabling room temperature sodium metal batteries. *Nano Energy* **2016**, *30*, 825–830. [[CrossRef](#)]
68. Iermakova, D.I.; Dugas, R.; Palacin, M.R.; Ponrouch, A. On the Comparative Stability of Li and Na Metal Anode Interfaces in Conventional Alkyl Carbonate Electrolytes. *J. Electrochem. Soc.* **2015**, *162*, A7060–A7066. [[CrossRef](#)]
69. Rodriguez, R.; Loeffler, K.E.; Nathan, S.S.; Sheavly, J.K.; Dolocan, A.; Heller, A.; Mullins, C.B. In Situ Optical Imaging of Sodium Electrodeposition: Effects of Fluoroethylene Carbonate. *ACS Energy Lett.* **2017**, *2*, 2051–2057. [[CrossRef](#)]
70. Lee, Y.; Lee, J.; Lee, J.; Kim, K.; Cha, A.; Kang, S.; Wi, T.; Kang, S.J.; Lee, H.W.; Choi, N.S. Fluoroethylene Carbonate-Based Electrolyte with 1 M Sodium Bis(fluorosulfonyl)imide Enables High-Performance Sodium Metal Electrodes. *ACS Appl. Mater. Interfaces* **2018**, *10*, 15270–15280. [[CrossRef](#)]
71. Chen, X.; Shen, X.; Hou, T.Z.; Zhang, R.; Peng, H.J.; Zhang, Q. Ion-Solvent Chemistry-Inspired Cation-Additive Strategy to Stabilize Electrolytes for Sodium-Metal Batteries. *Chem-US* **2020**, *6*, 2242–2256. [[CrossRef](#)]
72. Fang, W.; Jiang, H.; Zheng, Y.; Zheng, H.; Liang, X.; Sun, Y.; Chen, C.H.; Xiang, H.F. A bilayer interface formed in high concentration electrolyte with SbF₃ additive for long-cycle and high-rate sodium metal battery. *J. Power Sources* **2020**, *455*, 227956. [[CrossRef](#)]
73. Jiang, R.; Hong, L.; Liu, Y.C.; Wang, Y.D.; Patel, S.; Feng, X.Y.; Xiang, H.F. An acetamide additive stabilizing ultra-low concentration electrolyte for long-cycling and high-rate sodium metal battery. *Energy Storage Mater.* **2021**, *42*, 370–379. [[CrossRef](#)]
74. Zheng, X.Y.; Fu, H.Y.; Hu, C.C.; Xu, H.; Huang, Y.; Wen, J.Y.; Sun, H.B.; Luo, W.; Huang, Y.H. Toward a Stable Sodium Metal Anode in Carbonate Electrolyte: A Compact, Inorganic Alloy Interface. *J. Phys. Chem. Lett.* **2019**, *10*, 707–714. [[CrossRef](#)]

75. Kreissl, J.J.A.; Langsdorf, D.; Tkachenko, B.A.; Schreiner, P.R.; Janek, J.; Schroder, D. Incorporating Diamondoids as Electrolyte Additive in the Sodium Metal Anode to Mitigate Dendrite Growth. *ChemSusChem* **2020**, *13*, 2661–2670. [CrossRef]
76. Wang, H.; Wang, C.; Matios, E.; Li, W. Facile Stabilization of the Sodium Metal Anode with Additives: Unexpected Key Role of Sodium Polysulfide and Adverse Effect of Sodium Nitrate. *Angew. Chem. Int. Ed. Engl.* **2018**, *57*, 7734–7737. [CrossRef]
77. Yi, Q.; Lu, Y.; Sun, X.R.; Zhang, H.; Yu, H.L.; Sun, C.W. Fluorinated Ether Based Electrolyte Enabling Sodium-Metal Batteries with Exceptional Cycling Stability. *ACS Appl. Mater. Interfaces* **2019**, *11*, 46965–46972. [CrossRef]
78. Zheng, X.Y.; Gu, Z.Y.; Liu, X.Y.; Wang, Z.Q.; Wen, J.Y.; Wu, X.L.; Luo, W.; Huang, Y.H. Bridging the immiscibility of an all-fluoride fire extinguishant with highly-fluorinated electrolytes toward safe sodium metal batteries. *Energy Environ. Sci.* **2020**, *13*, 1788–1798. [CrossRef]
79. Liu, X.Y.; Zheng, X.Y.; Dai, Y.M.; Wu, W.Y.; Huang, Y.Y.; Fu, H.Y.; Huang, Y.H.; Luo, W. Fluoride-Rich Solid-Electrolyte-Interface Enabling Stable Sodium Metal Batteries in High-Safe Electrolytes. *Adv. Funct. Mater.* **2021**, *31*, 2103522. [CrossRef]
80. Doi, K.; Yamada, Y.; Okoshi, M.; Ono, J.; Chou, C.P.; Nakai, H.; Yamada, A. Reversible Sodium Metal Electrodes: Is Fluorine an Essential Interphasial Component? *Angew. Chem. Int. Ed.* **2019**, *58*, 8024–8028. [CrossRef]
81. Schafzahl, L.; Hanzu, I.; Wilkening, M.; Freunberger, S.A. An Electrolyte for Reversible Cycling of Sodium Metal and Intercalation Compounds. *ChemSusChem* **2017**, *10*, 401–408. [CrossRef] [PubMed]
82. Wang, S.Y.; Chen, Y.W.; Jie, Y.L.; Lang, S.Y.; Song, J.H.; Lei, Z.W.; Wang, S.; Ren, X.D.; Wang, D.; Li, X.L.; et al. Stable Sodium Metal Batteries via Manipulation of Electrolyte Solvation Structure. *Small Methods* **2020**, *4*, 1900856. [CrossRef]
83. Le, P.M.L.; Vo, T.D.; Pan, H.L.; Jin, Y.; He, Y.; Cao, X.; Nguyen, H.V.; Engelhard, M.H.; Wang, C.M.; Xiao, J.; et al. Excellent Cycling Stability of Sodium Anode Enabled by a Stable Solid Electrolyte Interphase Formed in Ether-Based Electrolytes. *Adv. Funct. Mater.* **2020**, *30*, 2001151. [CrossRef]
84. Han, M.; Zhu, C.; Ma, T.; Pan, Z.; Tao, Z.; Chen, J. In situ atomic force microscopy study of nano–micro sodium deposition in ester-based electrolytes. *Chem. Commun.* **2018**, *54*, 2381–2384. [CrossRef]
85. Wang, S.; Cai, W.; Sun, Z.; Huang, F.; Jie, Y.; Liu, Y.; Chen, Y.; Peng, B.; Cao, R.; Zhang, G. Stable cycling of Na metal anodes in a carbonate electrolyte. *Chem. Commun.* **2019**, *55*, 14375–14378. [CrossRef] [PubMed]
86. Li, P.; Jiang, Z.; Huang, X.; Lu, X.; Xie, J.; Cheng, S. Nitrofullerene as an electrolyte-compatible additive for high-performance sodium metal batteries. *Nano Energy* **2021**, *89*, 106396. [CrossRef]
87. Li, P.; Huang, X.; Jiang, Z.; Zhang, H.; Yu, P.; Lu, X.; Xie, J. High-rate sodium metal batteries enabled by trifluormethylfullerene additive. *Nano Res.* **2022**, *15*, 7172–7179. [CrossRef]
88. Luo, J.; Zhang, Y.; Matios, E.; Wang, P.; Wang, C.; Xu, Y.; Hu, X.; Wang, H.; Li, B.; Li, W. Stabilizing Sodium Metal Anodes with Surfactant-Based Electrolytes and Unraveling the Atomic Structure of Interfaces by Cryo-TEM. *Nano Lett.* **2022**, *22*, 1382–1390. [CrossRef]
89. Zhu, M.; Li, L.; Zhang, Y.; Wu, K.; Yu, F.; Huang, Z.; Wang, G.; Li, J.; Wen, L.; Liu, H.-K. An in-situ formed stable interface layer for high-performance sodium metal anode in a non-flammable electrolyte. *Energy Storage Mater.* **2021**, *42*, 145–153. [CrossRef]
90. Lee, J.; Lee, Y.; Lee, J.; Lee, S.-M.; Choi, J.-H.; Kim, H.; Kwon, M.-S.; Kang, K.; Lee, K.T.; Choi, N.-S. Ultraconcentrated sodium bis (fluorosulfonyl) imide-based electrolytes for high-performance sodium metal batteries. *ACS Appl. Mater. Interfaces* **2017**, *9*, 3723–3732. [CrossRef]
91. Zheng, J.; Chen, S.; Zhao, W.; Song, J.; Engelhard, M.H.; Zhang, J.-G. Extremely stable sodium metal batteries enabled by localized high-concentration electrolytes. *ACS Energy Lett.* **2018**, *3*, 315–321. [CrossRef]
92. Niu, Y.-B.; Yin, Y.-X.; Wang, W.-P.; Wang, P.-F.; Ling, W.; Xiao, Y.; Guo, Y.-G. In situ copolymerized gel polymer electrolyte with cross-linked network for sodium-ion batteries. *CCS Chem.* **2020**, *2*, 589–597. [CrossRef]
93. Wang, Q.; Wang, H.; Wu, J.; Zhou, M.; Liu, W.; Zhou, H. Advanced electrolyte design for stable lithium metal anode: From liquid to solid. *Nano Energy* **2021**, *80*, 105516. [CrossRef]
94. Lin, X.; Yu, J.; Effat, M.B.; Zhou, G.; Robson, M.J.; Kwok, S.C.; Li, H.; Zhan, S.; Shang, Y.; Ciucci, F. Ultrathin and non-flammable dual-salt polymer electrolyte for high-energy-density lithium-metal battery. *Adv. Funct. Mater.* **2021**, *31*, 2010261. [CrossRef]
95. Ford, H.O.; Cui, C.; Schaefer, J.L. Comparison of single-ion conducting polymer gel electrolytes for sodium, potassium, and calcium batteries: Influence of polymer chemistry, cation identity, charge density, and solvent on conductivity. *Batteries* **2020**, *6*, 11. [CrossRef]
96. Zheng, Y.W.; Pan, Q.W.; Clites, M.; Byles, B.W.; Pomerantseva, E.; Li, C.Y. High-Capacity All-Solid-State Sodium Metal Battery with Hybrid Polymer Electrolytes. *Adv. Energy Mater.* **2018**, *8*, 1801885. [CrossRef]
97. Wang, P.; Zhang, H.R.; Chai, J.C.; Liu, T.M.; Hu, R.X.; Zhang, Z.H.; Li, G.C.; Cui, G.L. A novel single-ion conducting gel polymer electrolyte based on polymeric sodium tartaric acid borate for elevated-temperature sodium metal batteries. *Solid State Ion.* **2019**, *337*, 140–146. [CrossRef]
98. Sangeland, C.; Mogensen, R.; Brandell, D.; Mindemark, J. Stable Cycling of Sodium Metal All-Solid-State Batteries with Polycarbonate-Based Polymer Electrolytes. *ACS Appl. Polym. Mater.* **2019**, *1*, 825–832. [CrossRef]
99. Wen, P.; Lu, P.; Shi, X.; Yao, Y.; Shi, H.; Liu, H.; Yu, Y.; Wu, Z.S. Photopolymerized gel electrolyte with unprecedented room-temperature ionic conductivity for high-energy-density solid-state sodium metal batteries. *Adv. Energy Mater.* **2021**, *11*, 2002930. [CrossRef]
100. Zhang, Z.; Huang, Y.; Li, C.; Li, X. Metal–organic framework-supported poly (ethylene oxide) composite gel polymer electrolytes for high-performance lithium/sodium metal batteries. *ACS Appl. Mater. Interfaces* **2021**, *13*, 37262–37272. [CrossRef]

101. Yang, J.F.; Zhang, M.; Chen, Z.; Du, X.F.; Huang, S.Q.; Tang, B.; Dong, T.T.; Wu, H.; Yu, Z.; Zhang, J.J.; et al. Flame-retardant quasi-solid polymer electrolyte enabling sodium metal batteries with highly safe characteristic and superior cycling stability. *Nano Res.* **2019**, *12*, 2230–2237. [CrossRef]
102. Luo, C.; Shen, T.; Ji, H.; Huang, D.; Liu, J.; Ke, B.; Wu, Y.; Chen, Y.; Yan, C. Mechanically robust gel polymer electrolyte for an ultrastable sodium metal battery. *Small* **2020**, *16*, 1906208. [CrossRef] [PubMed]
103. Wang, J.; Ni, Y.; Liu, J.; Lu, Y.; Zhang, K.; Niu, Z.; Chen, J. Room-Temperature Flexible Quasi-Solid-State Rechargeable Na-O₂ Batteries. *ACS Cent. Sci.* **2020**, *6*, 1955–1963. [CrossRef] [PubMed]
104. Yu, X.; Grundish, N.S.; Goodenough, J.B.; Manthiram, A. Ionic Liquid (IL) Laden Metal-Organic Framework (IL-MOF) Electrolyte for Quasi-Solid-State Sodium Batteries. *ACS Appl. Mater. Interfaces* **2021**, *13*, 24662–24669. [CrossRef] [PubMed]
105. Yang, L.; Jiang, Y.; Liang, X.; Lei, Y.; Yuan, T.; Lu, H.; Liu, Z.; Cao, Y.; Feng, J. Novel Sodium–poly (tartaric acid) borate-based single-ion conducting polymer electrolyte for sodium–metal batteries. *ACS Appl. Energy Mater.* **2020**, *3*, 10053–10060. [CrossRef]
106. Mendes, T.C.; Zhang, X.; Wu, Y.; Howlett, P.C.; Forsyth, M.; Macfarlane, D.R. Supported ionic liquid gel membrane electrolytes for a safe and flexible sodium metal battery. *ACS Sustain. Chem. Eng.* **2019**, *7*, 3722–3726. [CrossRef]
107. Zhang, C.; Hu, Q.; Shen, Y.; Liu, W. Fast-Charging Solid-State Lithium Metal Batteries: A Review. *Adv. Energy Sustain. Res.* **2022**, *3*, 2100203. [CrossRef]
108. Wang, C.; Liang, J.; Zhao, Y.; Zheng, M.; Li, X.; Sun, X. All-solid-state lithium batteries enabled by sulfide electrolytes: From fundamental research to practical engineering design. *Energy Environ. Sci.* **2021**, *14*, 2577–2619. [CrossRef]
109. Wang, C.; Liang, J.; Hwang, S.; Li, X.; Zhao, Y.; Adair, K.; Zhao, C.; Li, X.; Deng, S.; Lin, X.; et al. Unveiling the critical role of interfacial ionic conductivity in all-solid-state lithium batteries. *Nano Energy* **2020**, *72*, 104686. [CrossRef]
110. Wenzel, S.; Leichtweiss, T.; Weber, D.A.; Sann, J.; Zeier, W.G.; Janek, J. Interfacial Reactivity Benchmarking of the Sodium Ion Conductors Na₃PS₄ and Sodium beta-Alumina for Protected Sodium Metal Anodes and Sodium All-Solid-State Batteries. *ACS Appl. Mater. Interfaces* **2016**, *8*, 28216–28224. [CrossRef]
111. Wu, T.; Wen, Z.Y.; Sun, C.Z.; Wu, X.W.; Zhang, S.P.; Yang, J.H. Disordered carbon tubes based on cotton cloth for modulating interface impedance in beta''-Al₂O₃-based solid-state sodium metal batteries. *J. Mater. Chem. A* **2018**, *6*, 12623–12629. [CrossRef]
112. Deng, T.; Ji, X.; Zou, L.; Chikezzi, O.; Cao, L.; Fan, X.; Adegbisi, T.R.; Chang, H.-J.; Wang, H.; Li, B.; et al. Interfacial-engineering-enabled practical low-temperature sodium metal battery. *Nat. Nanotechnol.* **2022**, *17*, 269–277. [CrossRef] [PubMed]
113. Chi, X.; Hao, F.; Zhang, J.; Wu, X.; Zhang, Y.; Gheytani, S.; Wen, Z.; Yao, Y. A high-energy quinone-based all-solid-state sodium metal battery. *Nano Energy* **2019**, *62*, 718–724. [CrossRef]
114. Lei, D.; He, Y.-B.; Huang, H.; Yuan, Y.; Zhong, G.; Zhao, Q.; Hao, X.; Zhang, D.; Lai, C.; Zhang, S. Cross-linked beta alumina nanowires with compact gel polymer electrolyte coating for ultra-stable sodium metal battery. *Nat. Commun.* **2019**, *10*, 4244. [CrossRef]
115. Matios, E.; Wang, H.; Wang, C.L.; Hu, X.F.; Lu, X.; Luo, J.M.; Li, W.Y. Graphene Regulated Ceramic Electrolyte for Solid-State Sodium Metal Battery with Superior Electrochemical Stability. *ACS Appl. Mater. Interfaces* **2019**, *11*, 5064–5072. [CrossRef]
116. Ling, W.; Fu, N.; Yue, J.P.; Zeng, X.X.; Ma, Q.; Deng, Q.; Xiao, Y.; Wan, L.J.; Guo, Y.G.; Wu, X.W. A Flexible Solid Electrolyte with Multilayer Structure for Sodium Metal Batteries. *Adv. Energy Mater.* **2020**, *10*, 1903966. [CrossRef]
117. Yu, W.H.; Zhai, Y.F.; Yang, G.M.; Yao, J.Y.; Song, S.F.; Li, S.; Tang, W.P.; Hu, N.; Lu, L. A composite electrolyte with Na₃Zr₂Si₂PO₁₂ microtube for solid-state sodium–metal batteries. *Ceram. Int.* **2021**, *47*, 11156–11168. [CrossRef]
118. Zhao, Y.J.; Wang, C.Z.; Dai, Y.J.; Jin, H.B. Homogeneous Nat transfer dynamic at Na/Na₃Zr₂Si₂PO₁₂ interface for all solid-state sodium metal batteries. *Nano Energy* **2021**, *88*, 106293. [CrossRef]
119. Yang, J.Y.; Xu, H.H.; Wu, J.Y.; Gao, Z.H.; Hu, F.; Wei, Y.; Li, Y.Y.; Liu, D.Z.; Li, Z.; Huang, Y.H. Improving Na/Na₃Zr₂Si₂PO₁₂ Interface via SnO_x/Sn Film for High-Performance Solid-State Sodium Metal Batteries. *Small Methods* **2021**, *5*, 2100339. [CrossRef]
120. Wang, X.X.; Chen, J.J.; Mao, Z.Y.; Wang, D.J. In situ construction of a stable interface induced by the SnS₂ ultra-thin layer for dendrite restriction in a solid-state sodium metal battery. *J. Mater. Chem. A* **2021**, *9*, 16039–16045. [CrossRef]
121. Wang, C.Z.; Jin, H.B.; Zhao, Y.J. Surface Potential Regulation Realizing Stable Sodium/Na₃Zr₂Si₂PO₁₂ Interface for Room-Temperature Sodium Metal Batteries. *Small* **2021**, *17*, 2100974. [CrossRef]
122. Ruiz-Martinez, D.; Kovacs, A.; Gomez, R. Development of novel inorganic electrolytes for room temperature rechargeable sodium metal batteries. *Energy Environ. Sci.* **2017**, *10*, 1936–1941. [CrossRef]
123. Lin, X.T.; Sun, F.; Sun, Q.; Wang, S.Z.; Luo, J.; Zhao, C.T.; Yang, X.F.; Zhao, Y.; Wang, C.H.; Li, R.Y.; et al. O₂/O₂[−] Crossover- and Dendrite-Free Hybrid Solid-State Na-O₂ Batteries. *Chem. Mater.* **2019**, *31*, 9024–9031. [CrossRef]
124. Wu, S.; Qiao, Y.; Jiang, K.; He, Y.; Guo, S.; Zhou, H. Tailoring Sodium Anodes for Stable Sodium–Oxygen Batteries. *Adv. Funct. Mater.* **2018**, *28*, 1706374. [CrossRef]
125. Sun, Q.; Dai, L.; Tang, Y.F.; Sun, J.; Meng, W.D.; Luo, T.T.; Wang, L.; Liu, S. Designing a Novel Electrolyte Na_{3.2}Hf₂Si_{2.2}P_{0.8}O_{11.85}F_{0.3} for All-Solid-State Na-O₂ Batteries. *Small Methods* **2022**, *6*, 202200345. [CrossRef] [PubMed]
126. Liang, F.; Qiu, X.; Zhang, Q.; Kang, Y.; Koo, A.; Hayashi, K.; Chen, K.; Xue, D.; Hui, K.N.; Yadegari, H.; et al. A liquid anode for rechargeable sodium-air batteries with low voltage gap and high safety. *Nano Energy* **2018**, *49*, 574–579. [CrossRef]
127. Wang, C.; Deng, T.; Fan, X.; Zheng, M.; Yu, R.; Lu, Q.; Duan, H.; Huang, H.; Wang, C.; Sun, X. Identifying soft breakdown in all-solid-state lithium battery. *Joule* **2022**, *6*, 1770–1781. [CrossRef]
128. Song, S.; Kotobuki, M.; Zheng, F.; Xu, C.; Savilov, S.V.; Hu, N.; Lu, L.; Wang, Y.; Li, W.D.Z. A hybrid polymer/oxide/ionic-liquid solid electrolyte for Na-metal batteries. *J. Mater. Chem. A* **2017**, *5*, 6424–6431. [CrossRef]

129. Yang, J.; Gao, Z.; Ferber, T.; Zhang, H.; Guhl, C.; Yang, L.; Li, Y.; Deng, Z.; Liu, P.; Cheng, C. Guided-formation of a favorable interface for stabilizing Na metal solid-state batteries. *J. Mater. Chem. A* **2020**, *8*, 7828–7835. [[CrossRef](#)]
130. Lu, Y.; Alonso, J.A.; Yi, Q.; Lu, L.; Wang, Z.L.; Sun, C. A high-performance monolithic solid-state sodium battery with Ca^{2+} doped $\text{Na}_3\text{Zr}_2\text{Si}_2\text{PO}_{12}$ electrolyte. *Adv. Energy Mater.* **2019**, *9*, 1901205. [[CrossRef](#)]
131. Miao, X.; Di, H.; Ge, X.; Zhao, D.; Wang, P.; Wang, R.; Wang, C.; Yin, L. AlF_3 -modified anode-electrolyte interface for effective Na dendrites restriction in NASICON-based solid-state electrolyte. *Energy Storage Mater.* **2020**, *30*, 170–178. [[CrossRef](#)]
132. Chen, S.; Niu, C.; Lee, H.; Li, Q.; Yu, L.; Xu, W.; Zhang, J.-G.; Dufek, E.J.; Whittingham, M.S.; Meng, S.; et al. Critical Parameters for Evaluating Coin Cells and Pouch Cells of Rechargeable Li-Metal Batteries. *Joule* **2019**, *3*, 1094–1105. [[CrossRef](#)]
133. Chen, H.; Yang, Y.; Boyle, D.T.; Jeong, Y.K.; Xu, R.; de Vasconcelos, L.S.; Huang, Z.; Wang, H.; Wang, H.; Huang, W.; et al. Free-standing ultrathin lithium metal-graphene oxide host foils with controllable thickness for lithium batteries. *Nat. Energy* **2021**, *6*, 790–798. [[CrossRef](#)]
134. Niu, C.; Liu, D.; Lochala, J.A.; Anderson, C.S.; Cao, X.; Gross, M.E.; Xu, W.; Zhang, J.-G.; Whittingham, M.S.; Xiao, J.; et al. Balancing interfacial reactions to achieve long cycle life in high-energy lithium metal batteries. *Nat. Energy* **2021**, *6*, 723–732. [[CrossRef](#)]